

Modelling and Simulation of Keep-Lane Errors in Automated Vehicles

Faculty of Electrical Engineering and Information Technology

Master thesis in
Automated Driving and Vehicle Safety

BMW AG

Matrikel-Nr. 00119616

born in 19.09.1996 in Chidambaram

Sintpertstraße 46
81539 Munich

Supervisor: Dr.-Ing Ludwig Drees, BMW AG

Examiner: Prof. Dr.-Ing. Werner Huber, THI
Prof. Dr. rer. nat. Martin Ebert, THI

Start of thesis: 07.11.2022

End of thesis: 21.06.2023

Date of Presentation: 21.06.2023

Abstract

With the perpetual advancements in the field of automated driving, the first and foremost concern with regard to the acceptance of the technology by the general public is safety assurance. Safety assurance can only be established by displaying the consistency and reliability of the technology, proving that the manufacturer has taken all possible actions to mitigate the failures that might arise from the uncertainties and randomness that are introduced into the system. Statistical quantification of risks arising from potential failures is a proven metric for safety conformity as well as to determine acceptable safety levels. This thesis focuses on determining the overall injury risk by simulation of lane-keeping failure in an automated vehicle. A highly parameterized traffic model capable of simulating the interactive behavior of the automated vehicle along with other road users in normal highway traffic conditions is described in this thesis work. The overall injury risk is then determined by simulating the parameterized traffic model based on Monte Carlo simulation methodology, such that the traffic model can simulate the failure in nearly every possible traffic scenario, in concurrence with the likelihood of each state of the individual parameters that define a traffic scenario. Quantification of the risk of automated driving functions is important for safety validation, and it also provides statistically significant insights for defining the tolerable limits for a functional failure.

Acknowledgement

I would like to extend my deepest gratitude and appreciation to all the personages who have helped me in the successful completion of my master's thesis in collaboration with BMW AG. This research would not have been possible without the support, guidance, and encouragement from numerous individuals, and I am sincerely thankful for their invaluable contributions.

First and foremost, I would like to extend my heartfelt appreciation to my supervisor at BMW AG, Dr.-Ing Ludwig Drees. His expertise, insightful feedback, and continuous support throughout the entire research process have been instrumental in shaping the direction of this thesis. I am grateful for his patience, mentorship, and dedication to ensuring the quality and relevance of this work.

I would also like to extend my gratitude to the faculty members of Technische Hochschule Ingolstadt, Mr. Felix Fröhling, and Prof. Werner Huber, for their guidance and valuable input during the development of this research. Their extensive knowledge and expertise in the field have greatly enriched the content and methodology of this thesis. Their constructive criticism and attention to detail have been crucial in refining my ideas and enhancing the overall quality of this work.

I am indebted to the employees at BMW AG who generously shared their time, expertise, and resources, knowledge, enabling me to access crucial data and gain a deeper understanding of the subject matter. Their willingness to collaborate and their valuable insights have immensely contributed to the depth and practical relevance of this thesis.

Thank you all for your unwavering support and for being an integral part of this journey.

Rajagopalan Kannan

Contents

Abstract	I
Acknowledgement	II
Table of content	III
List of Figures	IV
List of Tables	V
Acronym	VI
1. Introduction	1
1.1. Motivation	1
1.2. Objective	2
1.3. Content and structure	2
2. Theoretical Background	1
2.1. Levels of vehicle automation	1
2.2. Errors in automated vehicles	1
2.3. Approval of automated vehicles	3
2.4. Functional safety of automated vehicles	4
2.5. Safety Of The Intended Function	5
2.5.1. Overview of Safety Of The Intended Function	5
2.5.2. Minimum Endogenous Mortality	6
2.5.3. Positive risk balance	7
2.6. Stochastic in automated driving	8
2.6.1. Importance of stochastic and statistics	8
2.6.2. Monte Carlo simulation	8
2.6.2.1. Overview of Monte Carlo simulation	8
2.6.2.2. Monte Carlo integration	9
2.6.2.3. Monte Carlo simulation in SOTIF analysis	10
2.7. Injury severity and collision types	11
2.7.1. Injury severity classification	11
2.7.2. Collision types	12
3. Methodology	1
3.1. Function description	1
3.1.1. Operating Design Domain	1
3.1.2. Scope of the study	1

3.2. Influential factors for injury risk	2
3.3. Traffic model	4
3.3.1. Assumptions	4
3.3.2. Input parameters	5
3.3.3. Model description	6
3.3.4. Initial position calculation	8
3.3.5. Maximum permissible lateral drift due to KLE	9
3.3.6. Trajectory tracking	11
3.3.7. Collision detection	13
3.3.8. Traffic participants' controllability	15
3.3.8.1. Braking intervention of the road users	15
3.3.8.2. Relative positioning between the vehicles	16
3.3.8.3. Avoid Side Collision	18
3.3.8.4. Neighbor vehicle braking	20
3.3.9. Classification of collision	21
3.3.10. Injury risk estimation	23
4. Data Sources	1
4.1. Ambient characteristics parameters	1
4.2. Ego characteristics parameters	4
4.3. Neighbor characteristics parameters	6
5. Results and Discussion	1
5.1. Traffic model simulation	1
5.1.1. Traffic model simulation overview	1
5.1.2. Traffic model visualization	2
5.2. Simulation results	3
5.3. Discussion	5
5.3.1. Injury risk Vs $v_{0, E}$	5
5.3.2. Injury risk Vs f_{KLE}	6
5.3.3. Injury risk Vs t_{KLE}	7
5.3.4. Injury risk Vs r_{KLE}	8
5.3.5. Injury risk Vs $t_{HW, \beta}$	9
6. Conclusion and Future work	1
6.1. Conclusion	1
6.2. Future work	2
Bibliography	VII
A. Appendix	VIII

List of Figures

2.1. Automated vehicle system architecture modules	2
2.2. Illustration of different types of collision	12
3.1. Factors that influence the collision in a simulation	2
3.2. Depiction of highway traffic model	4
3.3. Input parameters for highway traffic model	6
3.4. Traffic model concept	7
3.5. Illustration of emergency corridor in multi-laned roads	8
3.6. Intersection of the host vehicle's path with the road curvature	10
3.7. Trajectory of vehicle center	12
3.8. Illustration of separating axis theorem	15
3.9. Relative distances between the vehicles	17
3.10. Position and orientation of vehicles before collision	22
4.1. Road curvature distribution	1
4.2. Velocity distribution of the host vehicle	5
4.3. Distribution of distance to the vehicle ahead as a measure of time headway	7
4.4. Estimated gamma distribution for driver brake reaction time	9
5.1. Workflow of the traffic simulation model	1
5.2. Traffic simulation model visualization in MATLAB	2
5.3. Velocity of the vehicle during simulation	3
5.4. Convergence of MCS	3
5.4. Convergence of MCS (conti.)	4
5.5. Injury risk trend with vehicle velocity	5
5.5. Injury risk trend with vehicle velocity (conti.)	6
5.6. Injury risk trend with KLE occurrence rate	7
5.7. Injury risk trend with KLE duration	7
5.8. Injury risk trend with KLE drift radius	8
5.9. Injury risk trend with KLE duration	9

List of Tables

2.1. Injury severity mapping for different classifications	11
3.1. The resultant drift direction due to road and KLE curvature	9
3.2. Risk factors and the corresponding coefficient for the IRF	24
3.3. Shift in deltaV for IL1+ and IL3+ IRFs	24
3.4. Parameters of IRF for collision with pedestrians	25
3.5. Injury probabilities for different collisions	25
3.6. Possible collision outcome cases	26
3.7. Sub-categories for collision with road edge hazards	26
3.8. Road edge hazard occurrence rates	27
4.1. Sampling of road curvature	2
4.2. Likelihood of number of lanes in a scenario	2
4.3. Likelihood lane width for a scenario	2
4.4. Distance between the lane edge and road edge	3
4.5. Driving Mode	3
4.6. Sampling of KLE drift radius and drift duration	6
4.7. Likelihood of neighbor vehicle type	6
4.8. Dimensions of different vehicle types	7
5.1. Traffic model simulation results	4
A.1. Relative velocity likelihood matrix	IX

Acronym

KLE Keep Lane Error

PoRiBa Positive Risk Balance

AD Automated Driving

ODD Operating Design Domain

SAE Society of Automotive Engineers

NHTSA National Highway Traffic Safety Administration

L3 Function SAE Automation Level 3 Driving Function

ASC Avoid Side Collision

MCS Monte Carlo simulation

SOTIF Safety Of The Intended Function

HARA Hazard and Risk Analysis

ASIL Automotive Safety Integrity Level

MEM Minimum Endogenous Mortality

ISO International Organization for Standardization

L2- Automation Level 2 and below

L3+ Automation Level 3 and above

AI Artificial Intelligence

IRF Injury Risk Function

NASS National Automotive Sampling System

GIDAS German In-Depth Accident Study

SUMO Simulation of Urban Mobility

DLR German Aerospace Center

MAIS Maximum Abbreviated Injury Scale

Destatis Federal Statistical Office of Germany

MCI Monte Carlo integration

AIS Abbreviated Injury Scale

ISS Injury Severity Score

1. Introduction

In this introductory chapter, the objective behind the thesis and the overall approach is described. The motivation is presented first, followed by the objective, and then the chapter concludes with the structure outline of the thesis.

1.1. Motivation

Automated Driving (AD) technology has made significant advancements over the recent years [1]. Among the numerous motivations for its development and deployment, the most important ones are improving road safety, enhancing the traffic flow, and increasing accessibility and mobility to individuals with limited conventional mobility opportunities.

According to a study conducted by the National Highway Traffic Safety Administration (NHTSA), more than 90% of accidents on the roads are due to human error [2]. AD function has the potential to eliminate or lower human error, which reduces the number of accidents on the road. A recent study by the RAND Corporation [3] had published that with the AD functions over the next few decades an estimation of about 300,000 deaths can be prevented. Research has also shown that AD technology can improve the efficiency of traffic flow thereby lowering traffic congestion. As per a study conducted by the University of Texas at Austin [4], with a mere 10% of total cars on the roads having AD technology it could reduce traffic congestion by up to 40%. Apart from this, AD technology can also optimize fuel consumption by eliminating and or reducing unnecessary acceleration and braking, which lowers the fuel consumption and emissions [5]. Moreover, the introduction of self-driving cars could potentially provide mobility opportunities to people who are unable to drive, including the elderly, people with disabilities, and low-income individuals.

The key challenge for the development and testing of AD technology [6], is ensuring its safety and reliability as the function must be able to operate safely in all possible scenarios even during partial or complete failure of the function. Therefore, as a solution scenario-based testing is developed which is a very effective testing methodology [7], that focuses on verifying the safety of the AD function virtually during potentially hazardous scenarios that might arise in the real world during the operation of the AD function and cataloging both the results and test cases. Generally, multiple supporting functions are required for AD technology, so the safety and reliability of AD technology is dependent on the same for the supporting functions. One of the most fundamental and important functionalities of AD technology is the lane-keeping functionality. This ensures the safety of the passengers and other road users by maintaining the vehicle inside the lane while driving in autonomous driving mode. Lane-keeping is a complicated task, as it demands the vehicle to recognize and respond to the changes in the road

conditions such as curves, slopes, and obstacles. Thus, the lane-keeping functionality might have many unique challenges specific to different road types and driving scenarios.

Hence, the simulation of lane-keeping failure in AD function is a crucial step in evaluating the risk of AD function in normal driving conditions. The simulation aids in studying the behavior of the AD function and improving its robustness and reliability.

1.2. Objective

The main aim of this study is to assess the safety risk due to lane-keeping failure of the AD function as estimated injury probability. This is achieved in three parts: First, to create a mathematical model which represents the real-world behavior of the autonomous vehicle as well as the behavior of other traffic participants involved. Second, to simulate the AD function with lane-keeping failure in multiple discrete traffic scenarios using Monte Carlo simulation (MCS) methodology. Third, to quantify the risk in the form of injury probability for different injury levels that arise from the simulations.

1.3. Content and structure

A brief overview of the subject matter is provided in Chapter 1. The theoretical background regarding the subject matter is introduced in Chapter 2. The implementation and methodology of the study are discussed in Chapter 3. The source of the data set used in the study is described in detail in Chapter 4. Simulation results and inferences are discussed in Chapter 5. And finally, chapter 6 encapsulates the summary and subsequently gives a future outlook.

2. Theoretical Background

2.1. Levels of vehicle automation

Among the major trends reflecting the ongoing transformation of the automotive industry, autonomous driving continues to maintain a strong foothold in both its development and research endeavors. Automation in vehicles refers to the extent to which a vehicle can operate and manage its functions on its own without any human interventions. The Society of Automotive Engineers (SAE) has developed a widely recognized classification system for categorizing the different stages of vehicle automation into six systematic levels with a standardized framework that defines the capabilities and limitations of automated vehicles [8, 9].

- *Level 0 - No Driving Automation:* All the responsibilities of the driving tasks are assumed by the human operator.
- *Level 1 - Driver Assistance:* The overall control of the vehicle lies with the human operator. However, the driving is assisted with the support of the automation system.
- *Level 2 - Partial Driving Automation:* A combination of multiple automated functions are utilized for partial automation of the driving task. Nevertheless, the human operator must still monitor the environment and control the overall driving task.
- *Level 3 - Conditional Driving Automation:* The driving tasks under defined operating conditions are performed by the automated function itself. However, the human operator must always be prepared to regain control of the vehicle upon request from the automated function.
- *Level 4 - High Driving Automation:* The automation system is capable of carrying out the complete driving operation under defined operating conditions without relying on the human operator to take back control. Nevertheless, the human operator may be able to operate the vehicle when desired.
- *Level 5 - Full Driving Automation:* The automation system is capable of operating by itself under all conditions without relying on the human operator. However, the human operator may be able to operate the vehicle when desired.

2.2. Errors in automated vehicles

Vehicle system architecture is responsible for the control and implementation of different levels of automation in the vehicle. An automated vehicle can be imagined as a cognitive technical system comprising of three main modules in its system architecture [10, 11], as shown in figure 2.1. The first module is for the perception of the environment with use of sensors. The second

module is for formulating the action plan for the vehicle based on the perceived environment. And finally, the third module is for controlling the vehicle components in order to carry out the formulated action.

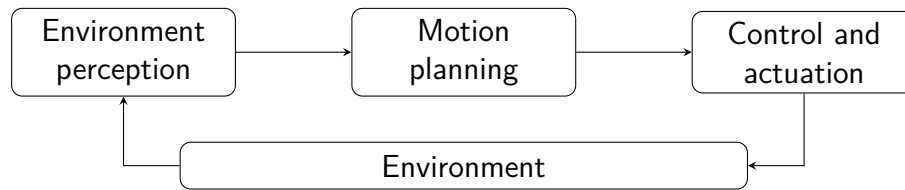


Figure 2.1.: Automated vehicle system architecture modules

As AD is achieved with the use of multiple autonomous techniques, the complexity of the function increases as well, potentially causing errors and failures that affect the system's stability, reliability, and safety. These issues must be resolved to mitigate and prevent any severe safety concerns for the vehicle. Thus, a detailed analysis of potential errors from AD technology is required to understand the present safety status. The errors from the AD technology for different automation levels are categorized based on the three broad components of the system architecture [6].

- *Perception error*: The environment perception module is responsible for the acquisition of sensor data about the surroundings to evaluate and formulate real-time action decisions. The advancements in AD technology are directly tied to the reliability, sustainability, complexity, and maturity of the sensing technology [12]. The three major sources of this error are hardware, software, and communication. Hardware error can arise from the degradation or failure of the sensors resulting in severe perception errors leading to unsafe driving operations. The malfunction of the software can also lead to a perception error. For vehicles with higher levels of automation, communication errors can occur during the transmission of data between the road and the vehicle and/or with other road users and/or with the cloud.
- *Decision error*: The motion planning module interprets the collected data from the perception level and formulates the next course of action. The decision errors are mainly due to system faults or human error. If the system algorithm is not able to effectively determine all the potential hazards before formulating the next action, the safety of the vehicle is compromised. In case of misjudgment by the system, the driver might require additional time to take full control of the vehicle due to preoccupation with a secondary task, thereby introducing uncertainties to the vehicle's safety. Thus, the availability of the driver must be factored in while designing the automated function to operate safely, even during a decision error arising from single or multiple functional failures.
- *Action error*: The action and control module is responsible to execute the formulated decisions from the motion planning module by controlling any and all of the vehicle

actuators: steering wheel, throttle valve, or brake. Additionally, the actuators are also monitored to confirm that the actions are executed and to formulate new deployment decisions. Action errors arise from the malfunctioning of the steering system, exhaust system, or power train which may threaten the safety of the vehicle. Human operators will be capable of sensing these errors and halting the driving operation in a very short response time. Therefore, the system must be designed to be able to detect the malfunction of the actuators and formulate actions to mitigate the effects of the malfunction on the driving operation.

2.3. Approval of automated vehicles

Owing to multiple decades of experience in the development of the automotive field, the industry and the regulatory bodies responsible for the validation and testing of the technology have acquired the expertise to develop safety standards and validation methodologies. However, these are majorly applicable to individual engineering components of the car as the development of highly automated driving functions is relatively recent in the history of the automotive industry. Thus, making the approval of the AD technology the most challenging aspect of its development. As the assessment and standardization of AD functions is a complicated process [13] which requires collaboration among system developers, regulatory authorities, and other stakeholders. The various steps involved in the approval of AD functions are development and testing, compliance of standards, type approval, operational approval, and continuous evaluation. The objective of the approval process is to ensure the safety, reliability, and functionality of the system are in accordance with requirements in order to assure the customer that the system is safe for usage.

Generally, AD functions have more than one objective, which includes, but is not limited to, the safety and comfort of the passengers. Validation and assessment of the comfort objectives are usually carried out with high reliability, either in a robust virtual environment or in a controlled testing facility. On the contrary, it is more challenging and complex to do the same for the safety objectives of the AD functions. The implementation of complicated active safety devices on the basis of engineering intuition and expert knowledge alone is neither cost-effective nor free of risk. The effectiveness of the safety feature of a particular AD function is usually difficult to be extracted from the corresponding accident statistics alone. Furthermore, the validation and evaluation of the safety feature based on accident statistics would require long periods of observation which leads to a lag between the development and optimization process in the V-model [14].

One of the most important differences with respect to the validation and approval between AD functions Automation Level 3 and above (L3+) and driver assistance functions Automation Level 2 and below (L2-) is the controllability and sudden intervention of the AD functions

over the course of its operation. The L2- functions restrain from unanticipated and abrupt interventions [15], as the focus of these L2- functions is to aid the driver who is primarily in control of the driving, unlike in L3+ functions where the system takes control of the driving task for a defined period of operation. The biggest challenge in the validation of AD function [16] is to prove that the safety level of automated driving is acceptable when in comparison with the current safety provided by human drivers.

Hazard and Risk Analysis (HARA) plays a major role in evaluating the safety and reliability of the AD functions and this in turn is also necessary for the definition of safety goals for the function. HARA involves a systematic evaluation of potential failure modes, testing the system's reliability, evaluating the reliability of individual components, and developing strategies to mitigate failures and ensure that the system operates safely and efficiently. By identifying and addressing potential issues proactively, reliability analysis will help to minimize the risk of accidents and build public trust in the technology. Thus, it is evident that both functional safety and safety of the intended function play a vital role in the testing and verification of the safety of the AD functions.

2.4. Functional safety of automated vehicles

Functional safety is undoubtedly crucial to the development, approval, and release of a new feature and/or function in a car, as it addresses and ensures the first and foremost requirement which is the safety of the usage of the product. Standards are drafted to provide guidelines, that can verify whether a product is capable of performing its functionality in a safe manner. As they establish requirements, specifications, recommendations, and characteristics in order to assure safety, reliability, and quality. International Organization for Standardization (ISO) developed ISO 26262, an automotive functional safety standard that is applicable to electrical and electronic systems comprising hardware and software components in vehicles. It defines the requirements and specifications to be met by the safety-relevant functions of all the electronic and electrical safety-related systems, as well as by processes, methodologies, and tools that are applied in the development process.

ISO 26262 standard is based on risk and the acceptance thereof. This standard establishes guidelines to identify and assess the risk of hazardous operational situations qualitatively. It also provides guidelines to define safety measures that can avoid and/or control systematic failures, detect and/or control random hardware failures, and mitigate their effects. The standard also defines automotive-specific risk classes Automotive Safety Integrity Level (ASIL), and provides guidelines for determining them based on the functionality of the system. On the basis of ASIL, the standard also establishes the necessary safety requirements of the system for achieving an acceptable residual risk. And most importantly it also provides guidelines to draft and define the requirements for validation, verification, and confirmation measures to

assure that an acceptable level of safety of the system is achieved.

The functional safety standard ISO 26262 is intended to stipulate the guidelines for hazard and risk mitigation arising from the malfunctioning of electrical and electronic safety-related systems, including the interaction within these systems. And as the standard does not stipulate and regulate the nominal working condition of the system, the ISO standard is applicable for any level of automated driving. However, in the context of the application of the standard to AD systems, the challenges of the ISO 26262 standard arise first and foremost due to the non-availability of the driver, as the driver will no longer be there to take over the control in case of a system failure in AD functions. Second, in the form of a semantic gap due to the complexity of the system because of a very high-level interconnection within the functions of the system. Third, on how to validate and test reliability, safety and security of the AD functions [17]. One of the contemporary approaches to reducing the function complexity is the model-based approach which provides a flexible mapping of hardware and software functions [18]. An iterative multi-level refinement was proposed to simplify the analysis in each step which thereby bridges the semantic gap [19].

2.5. Safety Of The Intended Function

2.5.1. Overview of Safety Of The Intended Function

Functional safety concerns and problems of driver assistance functions (L2-) are generally caused due to systematic failures or random hardware failures or uncertain input conditions. On the contrary, for AD functions (L3+) in addition to these failures, failures could also occur due to an uncertain output that is obtained due to the use of Artificial Intelligence (AI) algorithms. These uncertainties are unintended factors that can cause functional aberrations from the automotive applications and may also lead to unsafe situations and in turn lead to system failure. In general, the AI algorithms have a negative effect on the functional safety design, as the AI algorithms owing to their uncertainties may lead to unpredictable system failures, which in turn increases the vulnerability and risks of using these in the AD functions. To address the risk of failure due to functional insufficiencies of the intended functionality and/or foreseeable misuse of the function by the consumers, ISO had created a formal term Safety Of The Intended Function (SOTIF).

ISO 21448 is a standard that provides a framework and guidelines for the design, verification, and validation measures to prevent and avoid any hazardous risk arising from functional inadequacies such as the incompleteness of the specification of the intended function at a vehicle level or the incompleteness of specification and/or performance shortfall in the implementation of the electrical and electronic components of the system. In order to assure the safety of the intended function, any and all of the potential failure modes are addressed and the respective measures are taken in order to prevent and/or mitigate the risk emerging from the

potential failure hazards. This is very relevant since with the higher level of automated driving functions the responsibility for the safety of the complete driving activity will solely rest on the function and in turn on the system. Therefore, to comply with the safety norms there must be substantial evidence and also a validation methodology that can quantify the safety of the higher-level automated functions (L3+) both subjectively and objectively. ISO standards both ISO 26262 and ISO 21448 jointly provide guidelines to address the shortfalls of proving the safety of higher levels of driving automation (L3+).

The fundamental aim of SOTIF is to declare whether the indented function is safe by attempting to quantify the safety of the function. However, there exist undeniable technological gaps and challenges in the specification of the intended function requirements and in its verification at a system level. According to the generalized driving behavior proposed in [20] the important objective of the driver is to maintain a constant level of task difficulty throughout the driving activity wherein the task difficulty is objectively characterized based on the interdependent characteristics of the task demand and its execution capability. If the execution capability is more than the task demand the driving task difficulty is deemed as acceptable as it assures that the driving task at hand can be executed without any shortcomings.

The SOTIF requirements of L3+, as proposed in [21], can be verified by analyzing its operational scenarios and ensuring that the task difficulty of the driving activity by the system is acceptable. The SOTIF requirements are defined based on the worst-case situations and their corresponding severity in a predefined Operating Design Domain (ODD), where ODD of a function indicates where and when the function is operated [22]. Alternatively, the work of [23] suggests that a realistic estimation and determination of the vehicles' capability can be achieved via a scenario-based HARA that can combine both functional safety and SOTIF approaches to analyze the hazards. Risk evaluation and its acceptance thereof play an important role in SOTIF, because a function can be regarded as safe only when the risks arising from functional inefficiencies are lowered to a tolerable level. In general, the tolerable limits for risk from AD functions are very high. The road users, who are the traffic participants in a scenario including the automated vehicle, are the most influential stakeholder group in determining the risk tolerance for AD functions [24].

2.5.2. Minimum Endogenous Mortality

The Minimum Endogenous Mortality (MEM) is a risk acceptance principle that mandates that any new technology should not cause any significant increase in the individual risk when compared to the already existing MEM rate. The MEM rates for different groups of the general population are not the same and they are categorized based on the age of the group. The lowest endogenous mortality rate in western countries is $5 * 10^{-5}$ deaths per person per year, and they belong to children in the age group between 5 and 15 years old. It is prudent to note that these mortality rates are derived based on the data from the 1980s [25].

The present natural mortality rate in this modern world, as recommended in standards such as EN 50126, can however be extrapolated from these rates based on the assumption that an individual person is exposed to multiple systems (on an average 20) at the same time, resulting in the minimum mortality rate as $2 * 10^{-4}$ deaths per person per year [26]. Standard EN 50126, defines a significant increase as an increase of 5% in the MEM, about 10^{-6} deaths per person per year, and this is set as the absolute upper limit where the risks above them are considered to be unacceptable. Therefore, it can be concluded that MEM is used in the risk acceptance analysis especially while introducing a completely new technology into the market which is neither a replacement nor an extended version of the existing technology.

As MEM principle of risk acceptance sets an explicit target for the risk tolerance common across all industries it is proven to provide strong arguments and reasoning for setting the tolerance limit. Especially since the impact of a new technology is difficult to access before the launch a uniform risk tolerance makes MEM widely accepted in the automotive industry specifically in the context of automated driving.

2.5.3. Positive risk balance

The Positive Risk Balance (PoRiBa) principle was formulated based on the requirement drafted by the German Ethics Commission for automated and connected driving: “The objective is to reduce the level of harm until it is completely prevented. The licensing of automated systems is not justifiable unless it promises to produce at least a diminution in harm compared with human driving, in other words, a positive balance of risks.” [27]. The approach described in [28], aims to provide a qualitative risk-benefit framework for the automotive industry which can provide proof of reduction in the risk of automated vehicles in comparison with the existing human driving performance, which is adapted from the similar structured procedure in the pharmaceutical sector called PROACT-URL.

The objective of PoRiBa is to create an acceptance of the AD functions by both the general public and the authorities and PoRiBa can be broadly grouped into three parts. The first part is safety as a measurement, which refers to the different methods that can prove the balance of risks both quantitatively and qualitatively. The second part is safety as a threshold, which refers to determining a threshold for safety using the concepts of risk acceptance principles [29] to objectively determine if the risk balance is positive. The third part is safety as a process, which refers to the fostering of a safety culture within the organization such that the processes practiced in the organization are already proof of the required standards.

From the PoRiBa framework established in [28], it is evident that the assurance of risk balance only at the end of the development doesn't suffice, but rather it should be assured throughout the development process from the beginning up until the release of the product.

2.6. Stochastic in automated driving

2.6.1. Importance of stochastic and statistics

A stochastic process in probability theory is a mathematical object that is defined as a collection of random variables observed in a common probability space. It can be used to represent the random evolution or change of a system [30]. There have been numerous studies aiming to quantify traffic behavior in stochastic terms for highly immersive virtual simulations and virtual validation techniques. For instance, Simulation of Urban Mobility (SUMO), developed by the German Aerospace Center (DLR), exploits the stochastic behavior of urban traffic to conduct simulations that closely resemble reality. These simulations can be further utilized for virtual validation and/or monitoring [31].

The importance of statistics has increased significantly in the automotive industry, especially with the growth of AD technology. The statistical analysis [32] plays a vital role in enabling engineers to infer meaningful insights from data, evaluate functional performance, and assist in making reliable decisions. The study from [33] emphasizes the importance of statistical methods in evaluating the safety performance of automated driving technologies. Statistical models and techniques enable determining the performance metrics, analyzing the different potential failure modes, and in turn, evaluating the safety risk assessment. Thus, incorporating the statistical insights from the concept phase will lead to the development of robust and reliable automated driving systems.

The backbone of AD technology is built upon the integration of multiple sensors, intricate algorithms, and decision-making processes. Uncertainties and randomness are inherently introduced into the system warranting for its necessity to be addressed during the safety validation of the function. MCS is one of the prominent statistical techniques that ventures a unified approach to engulf the stochastic nature of traffic atop the inherent uncertainties to validate the safety of AD technology.

2.6.2. Monte Carlo simulation

2.6.2.1. Overview of Monte Carlo simulation

Monte Carlo simulation, also known as Monte Carlo Method or multiple probability simulation, is a powerful statistical technique used to model and estimate the possible outcomes of an uncertain event. The fundamental principle of MCS is based on ergodicity, which describes the statistical behavior of a moving point in an enclosed system following either a discrete time-dependent path or a randomized path. The moving point will eventually pass through all the parts of the enclosed space. MCS simulates complex systems using multiple random sampling such that all possible outcomes along with the individual probability of each outcome are obtained.

2.6.2.2. Monte Carlo integration

One of the most common applications of MCS is the Monte Carlo integration (MCI), whose objective is to estimate the integration of high dimension functions. Instead of relying on the discretization of the function for determining its integral as employed in the conventional numerical approach, MCI uses random sampling to estimate the integral of a function as the mean expected value of a random variable.

The fundamental principle of Monte Carlo integration is to evaluate the function at different randomly generated points within the integration domain [34]. The estimated integral value is determined by taking the average of the function values and scaling them by the size of the integration domain. For further understanding, a definite integral of a function $f(x)$ over a closed interval $[a, b]$ is considered as shown in equation 2.1.

$$I = \int_a^b f(x) dx \quad (2.1)$$

To approximate the integral function in equation 2.1 using MCI, firstly N_s random points, x_i , are generated between the interval $[a, b]$. And the function is evaluated at each of the random points and scaled based on the integration domain as shown in equation 2.2. From the law of large numbers, it is inferred that with the increase in the number of samples the expected value of a random variable approaches its empirical mean.

$$\hat{I}_{N_s} \approx \frac{b-a}{N_s} \sum_{i=1}^{N_s} f(x_i) \quad (2.2)$$

The bias of the result from MCI is zero, as the result is the mean expected value of an estimator. The variance of the result is dependent on the number of random sample points, as given in equation 2.3. Therefore, it can be inferred that the variance of results, in turn, the precision from MCS, is dependent on the number of random sample points generated.

$$\begin{aligned} Var(\hat{I}_{N_s}) &= Var\left(\frac{1}{N_s} \sum_{i=1}^{N_s} f(x_i)\right) = \frac{1}{N_s^2} Var\left(\sum_{i=1}^{N_s} f(x_i)\right) = \frac{1}{N_s} Var(f(x)) \\ &\left\{ Var(ax) = a^2 Var(x) \quad \& \quad Var(x+y) = Var(x) + Var(y) \right\} \end{aligned} \quad (2.3)$$

The biggest advantage of MCI is its ability to handle complex functions and high dimensional spaces, which are either computationally expensive or impractical using conventional methods. On the contrary, the shortfall of MCI is that the convergence rate of the solution is slower in comparison to other numerical methods. As precision in MCI is dependent on the number of samples, high precision demands a large number of simulation samples. Techniques such as importance sampling and stratified sampling have been developed to improve the convergence with the help of strategic statistical principles without the necessity to increase the number of random samples drastically.

In importance sampling instead of generating random samples from its corresponding distribution, rather it is sampled from a distinctive distribution function called importance distributions that generates sample points on the region of the distribution that has a strong contribution to the given problem. The results from the samples based on the importance distribution function are weighted by the importance factor to obtain the integral estimate. In this method, the variance of the result is reduced as more samples are generated in the significant region of the problem.

In stratified sampling, the integration domain is divided into smaller, equal-sized regions, and random samples are generated within each of these regions. Hence, as the name suggests even distribution of sample points across the integration domain are generated, which in turn improves the convergence and lowers the variance of the result.

2.6.2.3. Monte Carlo simulation in SOTIF analysis

The MCS technique innately incorporates randomness and uncertainty into its statistical framework while simulating and analyzing the behavior and performance of a system. In contrast to traditional testing methods, MCS proposes a systematic and probabilistic approach, aiming to generate scenario cases randomly from the complete range of possible scenarios. This approach attempts to capture most of the critical edge cases by accounting for various factors like sensor noise, environment conditions, and traffic patterns as input to the simulation.

By running multiple iterations of simulations with random inputs, MCS enables researchers and engineers to evaluate the performance and robustness of automated driving systems. It helps identify potential failure modes, assess risk factors, and optimize algorithms to enhance the vehicle's ability to handle challenging situations. Moreover, the statistical nature of Monte Carlo simulation provides valuable insights into the system's behavior and performance under different conditions, offering a more comprehensive understanding of the vehicle's capabilities and limitations.

An MCS model for any system comprises of four essential steps. The first step is to identify the transfer equation which can quantitatively represent the behavior of the system by means of mathematical expressions. The second step is to define the distributions of the input parameters to the simulation model. The input parameters are modelled as random variables with a probability distribution, considering the uncertainty and randomness of each parameter, instead of being modelled as deterministic values. The third step is to set up the simulation by preparing a large data set for each input parameter that is sampled at random. The fourth step is to analyze the final outcome of the simulation for each of the combinations of the input parameters, according to the transfer equations that represent the behavior of the system.

The framework represented in [35], can generate a probability distribution encompassing all

possible combinations of motions with reasoning for multiple objects, non-automated vehicles, and other road users in a road scene using MCS. Merely considering the distance between two objects on the road alone is not sufficient to conclude if the scenario is safe in the immediate future. Instead, the behavior of all road users is necessary. The proposed system predicts the best possible action based on the impact of predicted future motions on the vehicle under study as well as on the other vehicles.

MCS methodology can be employed for determining the occurrence and severity of scenario-specific hazards in order to quantify the risks for a particular scenario. The study carried out by [36] aimed to determine the severity and exposure of potential hazards for a vehicle operating under AD condition while experiencing a cut-in scenario. The input parameters MCS are marginalized to fit an estimated probability and then given as input to the simulation model. Based on the percentage of collision obtained from MCS and the exposure value of such a scenario, the collision risk is estimated.

2.7. Injury severity and collision types

2.7.1. Injury severity classification

The Abbreviated Injury Scale (AIS) [37], has been widely used for the classification of traumatic injuries, particularly those caused by automobile collisions by the Medical Engineering Accident Investigation Teams of the NHTSA, by the NATO Country Teams in Europe, etc. Injury Severity Score (ISS), [38, 39], is a quantitative methodology that describes the threat to human life arising from vehicle accidents based on its corresponding AIS injury scores. Injury severity levels in the automotive industry are generally categorized on the basis of Maximum Abbreviated Injury Scale (MAIS), which indicates the maximum value of all AIS scores, from all of the injuries. The different levels of injury severity according to different metric standards are listed in the table 2.1.

Injury severity level and definition	Severity scores		
	MAIS	Destatis	ISO
IL1 - Slight injury	AIS1 - AIS2	Leichtverletzte	S1
IL2 - Severe injury	AIS3 - AIS4	Schwerletzte	S2
IL3 - Fatal injury	AIS5 - AIS6	Getötete	S3

Table 2.1.: *Injury severity mapping for different classifications*

In any traffic simulation study, the most important measurement metric for safety is the injury estimation arising from the possible collisions in the simulations. Injury estimation of a collision is indicated as the probability of different injury levels arising from the collision, depending on the type of collision and the corresponding accident parameters, such as the colliding object, the impact velocity, the collision angle, and so on.

Injury Risk Function (IRF), [40], for a particular injury severity with a specific collision type indicates the probability trend of the particular injury severity with respect to important accident parameters, impact velocity is most commonly used for this purpose of indicating the probability trend. IRF is developed as a methodology to quantify the risk of collision, by mapping the likelihood of the injury severity with respect to its corresponding accident parameters. For each severity level specific to a particular collision type, a specific IRF is required to predict the injury probability.

2.7.2. Collision types

Generally, a road accident might involve multiple collisions and for the purpose of this thesis, a collision is defined as an instance where one vehicle is striking an obstacle or another vehicle thereby restricting the maximum number of vehicles involved in a collision to two. Collisions in road accidents are classified into different collision types based on the point of impact, the direction of the approaching vehicle, and finally the angle of collision. For collisions involving two vehicles, each vehicle can experience either the same or a different type of collision. The different types of collisions from the perspective of a single vehicle are illustrated in figure 2.2.

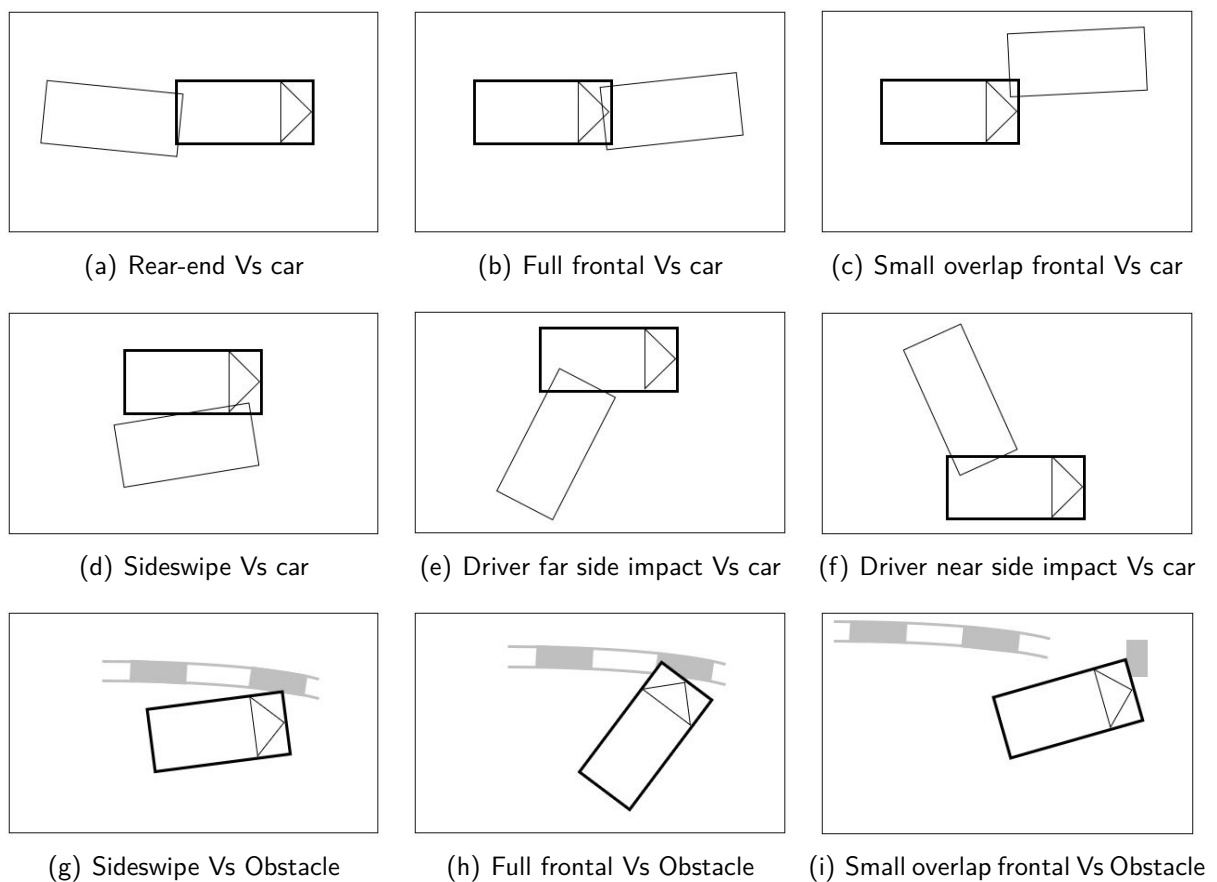


Figure 2.2.: *Illustration of different types of collision*

3. Methodology

3.1. Function description

3.1.1. Operating Design Domain

The safety of AD function that is assessed in this thesis work is SAE Automation Level 3 Driving Function (L3 Function). The vehicle under investigation, which is using the L3 Function, is henceforth regarded as the host vehicle or as Ego in this thesis work. The Operating Design Domain of the function, is assumed, without contradiction, to be between 1 to 60 kmph in highway traffic conditions. Two possible driving modes are available within the scope of the assumed ODD for the host vehicle, and it is dependent on the velocity of the host vehicle. The first mode is normal driving which is operated between 30 to a maximum of 60 kmph. The second mode is the emergency corridor maneuver, which is operated between 1 to a maximum of 30 kmph. Additionally, an inbuilt safety functionality Avoid Side Collision (ASC) is included in the L3 Function, which prevents the lateral collision of the host vehicle with the neighboring vehicle or lowers the impact thereof, by braking the host vehicle when the necessary braking conditions are satisfied.

3.1.2. Scope of the study

The aim of this study is to simulate the failure of lane-keeping functionality by introducing a Keep Lane Error (KLE) in the L3 Function and estimate the injury risk probabilities due to the collisions arising from the KLE. Lane-keeping error is introduced to the L3 Function as an involuntary lateral drift of the host vehicle having a constant turning radius. Collision avoidance measure limited to the scope of this study is only the braking of the neighboring vehicles and/or the host vehicle (as ASC functionality). Other collision avoidance maneuvers such as steering and acceleration are out of the scope of this study. The injury estimation of collision arising from KLE in this study is limited to a maximum of two vehicles - the host vehicle and the neighboring vehicle which with the host vehicle participates in the immediate collision alone. The impact of the collision on the remaining traffic participants is out of the scope of this study and their impact on the overall injury estimation is also out of the scope of this study.

The collisions in the simulation can be broadly categorized into two parts, collision of the host vehicle with another traffic participant and collision of the host vehicle with road edge obstacles or hazards. The different types of road users that are included in the scope of this study are cars, trucks/buses, and motorcycles. The different types of road edge hazards that are included in the scope of this study are trees, lamp-posts, guardrails, guardrail ramps, break-down vehicles, and pedestrians.

3.2. Influential factors for injury risk

In order to study in detail about injury risk of a scenario, the severity of the collision as well as the corresponding conditions which had consequently led to a collision must be examined closely. Therefore, the following section describes the different factors which are responsible for the occurrence of the collision and also the factors that decide the severity of the collision. A simple representation of the factors is shown in figure 3.1, where the factors on the left side influence the occurrence of the collision and the factors on the right side influence the severity of the collision.

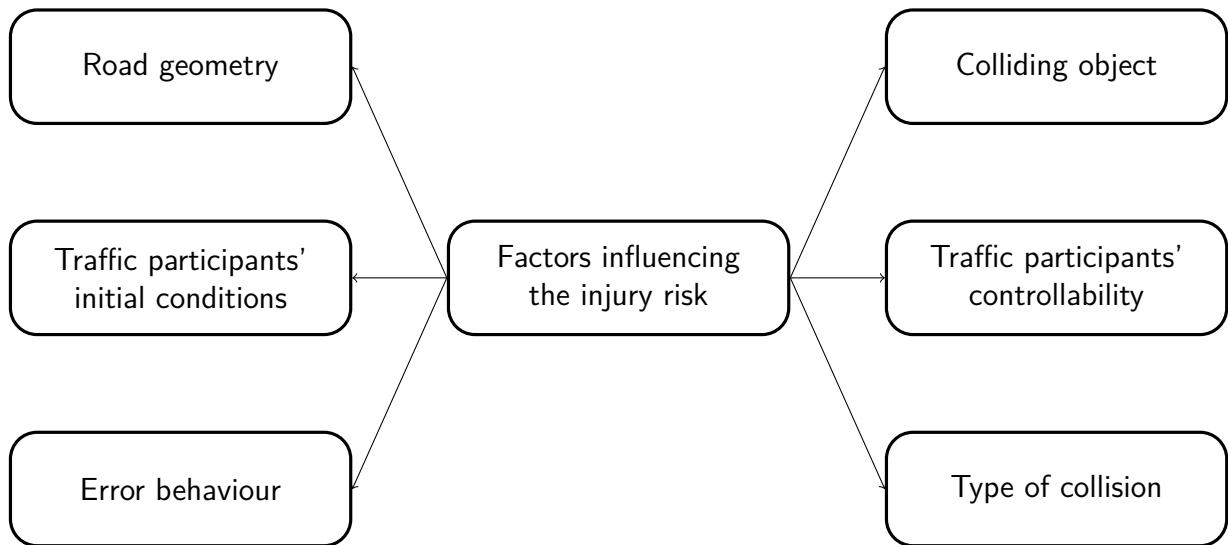


Figure 3.1.: *Factors that influence the collision in a simulation*

- *Road geometry* describes the different features of the road such as the width of the lane, number of lanes, curvature of the road, the distance of the guardrail from the end of the lane edge, etc, which are responsible for collisions in the simulation. Lane width will decide the lateral distance that is available for the host vehicle to drift until it crosses its own lane and invades the neighboring lane. The number of lanes along with the initial positioning of the host vehicle will decide the maximum lateral distance available for the host vehicle until the road edge. The curvature of the road is an essential factor to determine the deviation due to lane-keeping failure. The distance to the guardrail from the road edge is also important in determining the total plausible lateral drifting distance available for the host vehicle until it completely exits the road and collides with the guardrail or any other obstacle that may be present along the road edge.
- *Traffic participants' initial conditions* will decide both the nature and the type of collision of the host vehicle with another traffic participant. This entails the initial positioning, the initial velocity, and also the initial time headway to the next vehicle both for the host vehicle as well as for the neighboring vehicle in the simulation. The traffic density is a measure of indication of the degree of closeness of vehicles in a simulation and time headway is one of the most common means of indication of the traffic density along a

particular lane. The combination of the relative positioning and relative velocity of the neighboring vehicle with respect to the host vehicle is crucial to determine whether a collision is imminent, it is also necessary to determine whether the imminent collision will occur either with another traffic participant or with the road edge feature. Initial conditions of the traffic participants are also required to determine the exact instant in the simulation at which the imminent collision would occur.

- *KLE characteristic* is the most influential factor for the collision of the host vehicle which is operating under L3 Function. As this error triggers the vehicle under L3 Function to stray away from the intended safe path and cause the potential collision. KLE is very dynamic in nature and hence for simulation and modelling purposes, this error is assumed, without contradiction, to be a constant turn radius for a particular duration. The resulting collision due to the KLE is considered as the measure of the potential risk which would be caused by the failure of the lane-keeping functionality in the L3 Function. The KLE turn radius is independent of the curvature of the road and it is bidirectional in nature, meaning the host vehicle is expected to drift away from the intended path in both directions at a constant turning radius regardless of the road curvature throughout the simulation for a certain duration of time.
- *Colliding object* is one of the most vital aspects in determining the severity of the collision. The most important and crucial deciding factor in the estimation of the injury levels in case of a collision is delta-V. Delta-V is majorly dependent on the object type, because it is derived based on the conservation of momentum principle. The nature of the motion of the colliding object, that is whether the object is fixed or is in motion, along with the weight of the colliding object will affect the conservation of momentum principle which in turn affects the estimation of delta-V.
- *Traffic participants' controllability* plays a very important role in lowering and mitigating the effects of an imminent collision. Controllability measures considered in this study are the braking of the host vehicle due to the ASC functionality and the preventive braking of the neighboring vehicle because of a perceived danger arising from the lane intrusion of the host vehicle due to the KLE. This braking of the traffic participants can either completely avoid the imminent collision altogether or can lower the impact velocity, consequently the delta-V, and potentially delay the collision.
- *Type of collision* also plays an important role in deciding the severity of the collision. As the type of collision dictates exactly the effects of the collision on all of the vehicles involved in it, and thus it is essential to determine the type of collision in order to properly estimate the injury level of the collision. The different types of collisions that are considered in this study are head-on frontal collision, rear-end collision, far-side impact collision, near-side impact collision, small overlap or small offset frontal collision, and sideswipe collision. The collision type, together with the colliding object type and the impact velocity determines the overall estimation of the injury level.

3.3. Traffic model

This section will describe in detail the traffic model for an automated vehicle with lane-keeping failure in normal highway traffic conditions. A depiction of the highway traffic model is shown in figure 3.2. The figure represents a traffic scenario under normal highway traffic on a 3-lane-highway road, Where the road is curved to the right from the top view. The host vehicle is driven under L3 Function with a KLE forcing the host vehicle to turn to the left, from the top view, at a constant turn radius. The other traffic participants, i.e., neighboring vehicles, are driving along the curvature of the road without any deviation from the road curvature.

The simulation leads to the collision between the host vehicle and the neighboring vehicle as the host vehicle deviates from its path and enters into the neighboring vehicle's lane, i.e., drifting of the host vehicle from its initial position in lane 2 onto lane 3 due to KLE. The longitudinal direction of the vehicle is depicted along the horizontal direction (x-axis) and the lateral direction of the vehicle is depicted along the vertical direction (y-axis) in the model depiction.

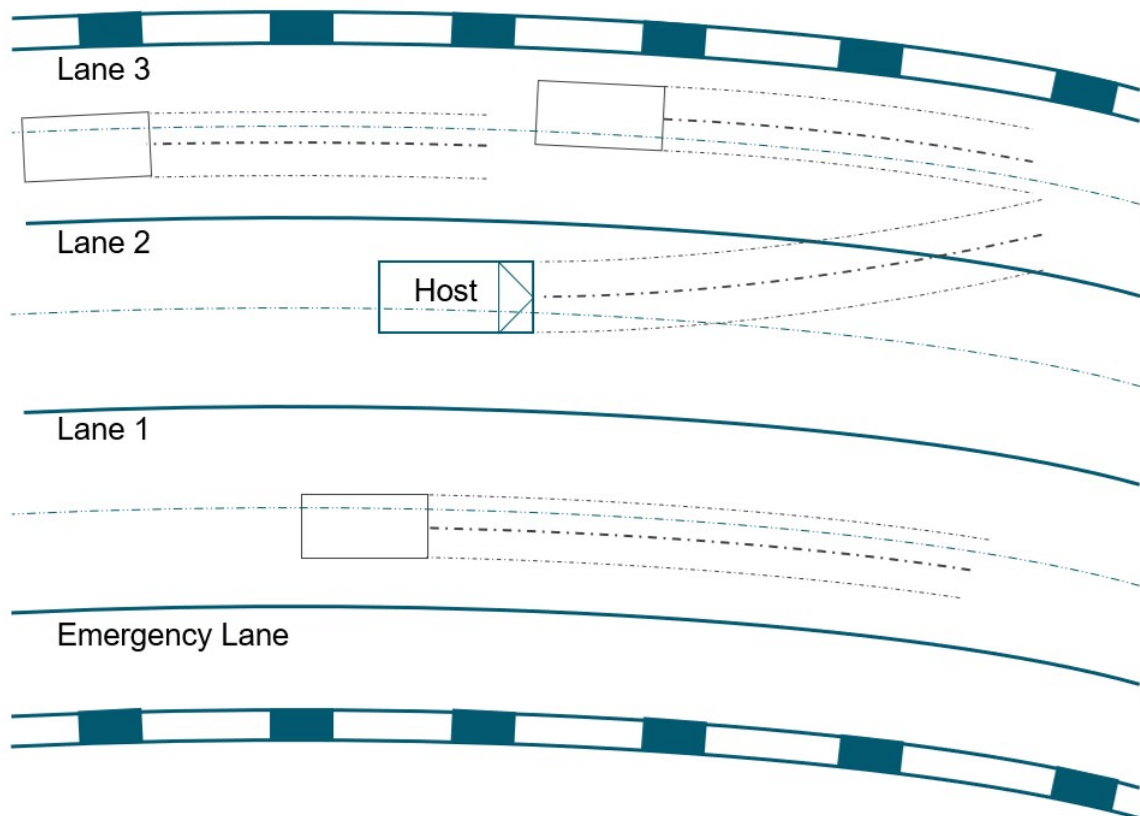


Figure 3.2.: *Depiction of highway traffic model*

3.3.1. Assumptions

In order to determine the reliability of the L3 Function, the first and foremost important assumption considered is that the failure of the L3 Function was caused only because of the

failure of one essential functionality of the L3 Function, which is the lane-keeping functionality. The remaining functionalities involved in the system during the operation of L3 Function are considered to be operating in perfect working condition. The sensory information that indicates the relative distance and relative velocity of the other traffic participants, i.e., the neighboring vehicles, are assumed to be accurate without any tolerance error.

The traffic model is simulated only from the beginning of the KLE either until the end of the error or until a collision occurs, whichever occurs earlier. The injury estimation of the collisions arising from the simulations is based on injury risk functions, which are models derived from prior literature reviews, and they are also assumed to be applicable and valid for this study.

It is also assumed in this study that the traffic participants are considered to have no change in acceleration throughout the simulation unless an appropriate response of braking is warranted by the neighbor due to the lane intrusion of the host vehicle and/or by the host vehicle when the conditions of the ASC are satisfied. Braking behavior in this model is considered to be constant, and the deceleration build-up time is neglected in this model. The road curvature is modelled to have a constant radius of curvature for each of the lanes in the model. Since the model is simulated only when a KLE occurs during the L3 Function, a conservative assumption of constant road geometry throughout the simulation is considered.

3.3.2. Input parameters

The traffic model in this study is developed for simulating a functional scenario in which the lane-keeping functionality fails in an automated vehicle operating in normal highway traffic conditions under L3 Function. The proposed traffic model is capable of simulating multiple concrete scenarios using the MCS methodology. A concrete scenario is described in detail with the help of scenario parameters which would be providing exact information and details that are essential to reconstruct the scenario in a virtual and or in a real environment for further research and validation.

The model input parameters that are required to derive further dependent model parameters that are essential for the description of the concrete scenarios of highway traffic scenarios are broadly categorized into three categories: ambient characteristics, ego characteristics, and neighbor vehicle characteristics. Parameters belonging to each of these categories are listed in figure 3.3. The description of these parameters and their influence on the traffic model is discussed further in this section. A detailed description of the model input parameters along with the distribution of the parameter states for each of the model parameters considered in this traffic model is elaborated in chapter 4.

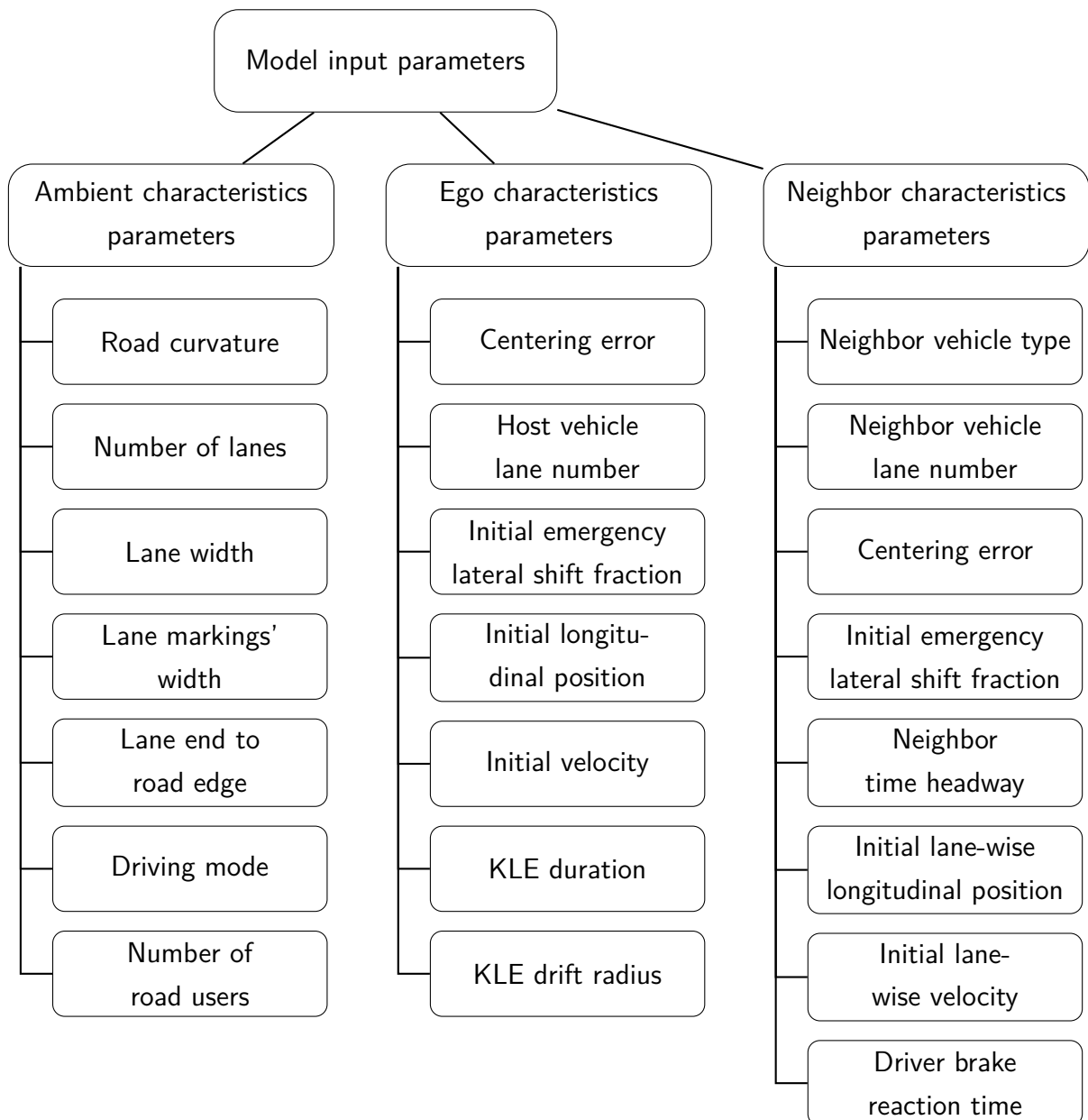


Figure 3.3.: *Input parameters for highway traffic model*

3.3.3. Model description

The traffic simulation model is built on an inertial reference frame X-Y as shown in figure 3.4, where the longitudinal measurement of the traffic scenario is along the X-axis and the lateral measurement is along the Y-axis. All the paths taken by the vehicles and the curvature of the road are depicted as circles, where the centers of all the curves lie along the Y-axis. The X-axis of the X-Y frame is positioned on the rightmost edge of the road lying on the Y-axis.

The positive values along the X-axis indicate longitudinal measurements along the direction of forward motion and vice versa for the negative values. Similarly, the positive values along the Y-axis indicate lateral measurements along a direction from the right side of the road to the left and vice versa for negative values.

The path of the host vehicle is controlled by the KLE drift radius, r_{KLE} , for a duration of t_{KLE} , and the path of the other vehicles are along the curvature of the road, r_{road} . The direction of the turn with respect to the X-Y frame is represented by the sign of the turn radius, where a right turn is indicated by a negative radius and a left turn by a positive radius value. The positions of the vehicles with respect to the inertial frame are not continuously determined, but discretely at the frequency of 10 Hz , i.e., the positions are determined for every tenth of a second implying that every instant of the simulation is $1/10^{th}$ of a second apart from one another.

The lane width of the road is represented as W_L and the lane markings' width is given by W_{LM} . For any vehicle in a scenario, β , the track width is indicated as TW_β and the wheel base is denoted as WB_β . The number of lanes in a scenario is denoted by n_{Lanes} , and the lane assigned to any vehicle is designated by $n_{Lane, \beta}$. The distance between the lane edge to the road edge from the leftmost lane is denoted by LTR_{left} and by LTR_{right} from the rightmost lane. Positions of all the vehicles in the proposed traffic model are indicated by the co-ordinates of their corresponding centers. The subscripts E & β denote the attributes of the host vehicle and neighbor vehicles respectively.

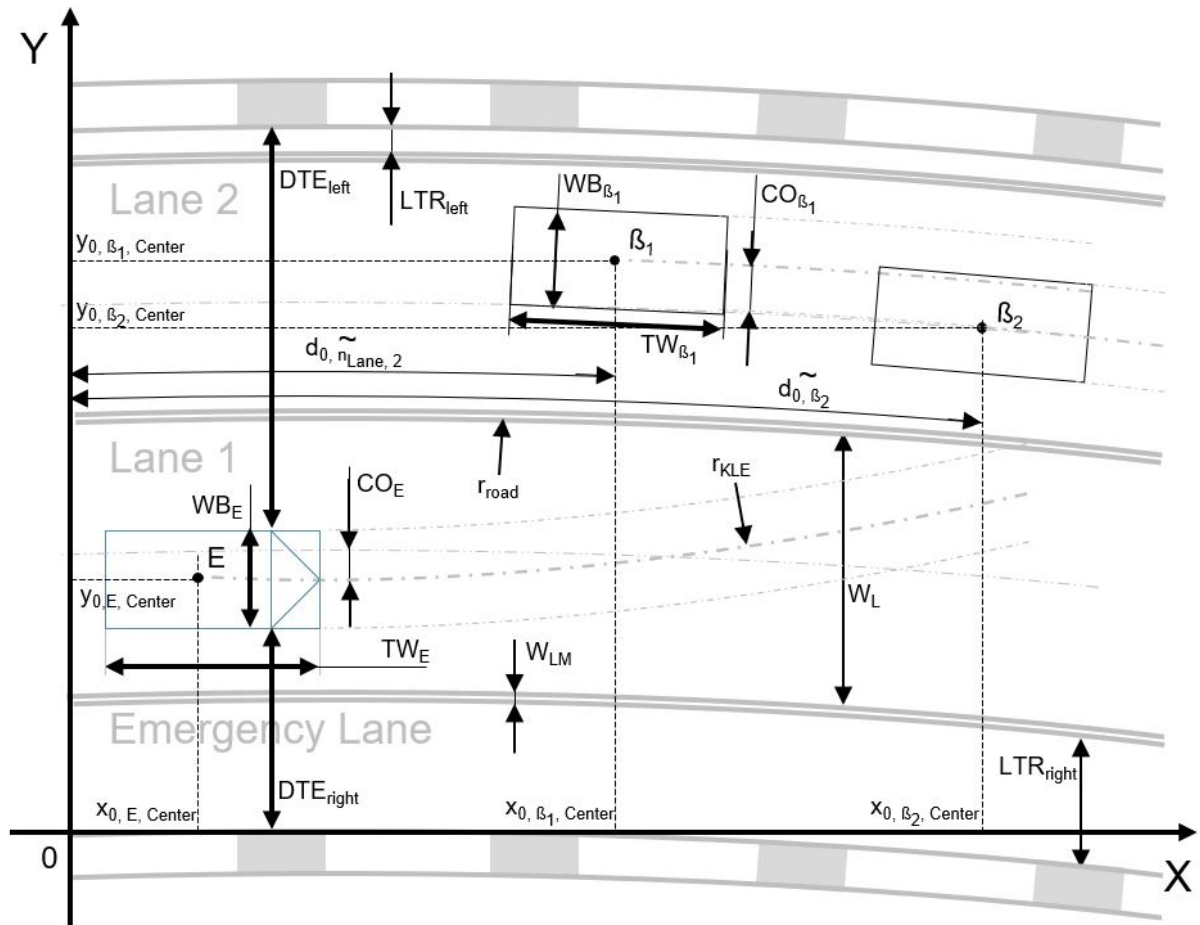


Figure 3.4.: Traffic model concept

3.3.4. Initial position calculation

Determining the starting positions of all the vehicles in the traffic model with respect to the inertial reference frame X-Y is the first and foremost step. Both the driving mode in the ODD of the L3 Function under study is incorporated in the proposed highway traffic model. Where $D_{Mode, EC}$ denotes the emergency corridor driving mode and $D_{Mode, ND}$ denotes the normal driving mode. The initial lateral positioning offset of the vehicles at the beginning of the simulation is dependent on the driving mode of the scenario and also on the lane assigned to the corresponding vehicle. The initial lateral offset of the vehicles due to the emergency corridor situation is as indicated in figure 3.5.

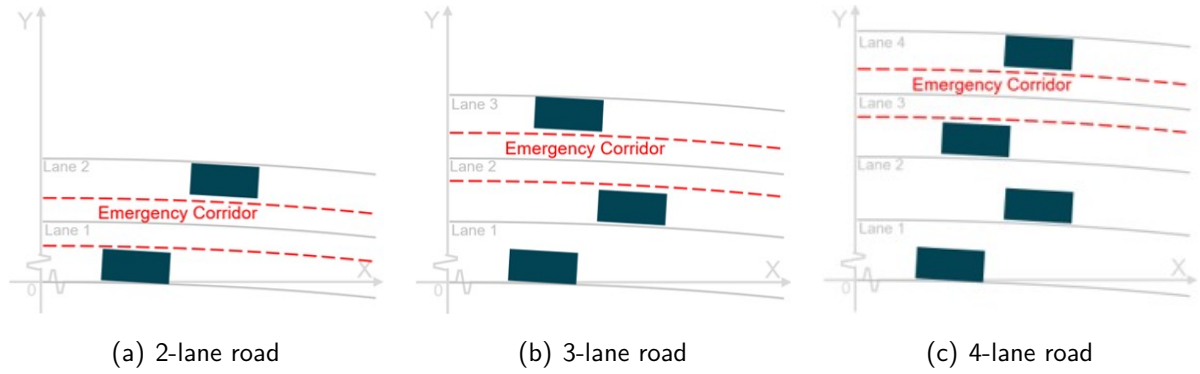


Figure 3.5.: Illustration of emergency corridor in multi-laned roads

As shown in equation 3.1, the initial lateral shift of each vehicle for emergency corridor maneuver, $y_{0, shift, \$}$, is influenced by a fraction of the initial emergency lateral shift, $perc_{shift_{\$}}$. And the corresponding lateral shifting side, $y_{0, shift, \$, side}$, is dependent on the lane to which the vehicle is assigned.

$$y_{0, shift, \$, side} = \begin{cases} -1, & \text{if } n_{Lane, \$} = n_{Lane} \\ +1, & \text{otherwise} \end{cases} \quad \{ \$ \in \text{All vehicles in the scenario} \} \quad (3.1)$$

$$y_{0, shift, \$} = \begin{cases} 0, & \text{if } D_{Mode, ND} \\ (W_L - TW_{\$}) * 0.5 * frac_{shift_{\$}} - 0.2, & \text{if } D_{Mode, EC} \end{cases}$$

The initial center-line offset, $CO_{\$}$, is the overall lateral offset of the vehicles at the start of the simulation. As given in equation 3.2, $CO_{\$}$ is influenced by the initial centering error, $C_{\$}$, and the initial lateral offset corresponding to the emergency corridor maneuver alone.

$$CO_{\$} = y_{0, shift, \$} * y_{0, shift, \$, side} + C_{\$} \quad (3.2)$$

From the center-line offset the initial lateral position of all the vehicles, $y_{0, \$}$ is calculated using equation 3.3.

$$y_{0, \$} = (n_{Lane, \$} - 0.5) * W_L + (n_{Lane, \$} * W_{LM}) + CO_{\$} \quad (3.3)$$

For a neighbor vehicle, β_q , designated to lane, n_{Lane, β_q} , with $q - 1$ vehicles behind it, the distance of its initial position from the Y-axis along the curvature of the road, d_{0, β_q} , is dependent on $d_{0, \beta_{q-1}}$, and $t_{HW, \beta_{q-1}}$ as given in equation 3.4. Where $d_{0, \beta_{q-1}}$ is the distance of the initial position of β_{q-1} , which is the vehicle immediately behind β_q in the same lane, from the Y-axis along the curvature of the curvature. And $t_{HW, \beta_{q-1}}$ denotes the time headway distance between β_{q-1} & β_q in seconds. In this traffic model, it is assumed, without any further contradiction, that the initial velocity of all the vehicles along a lane is the same. Therefore, the initial velocity of β_{q-1} is same as that of β_q which is v_{0, β_q} .

$$d_{0, \beta_q} = \begin{cases} d_{0, n_{Lane, l}}, & \text{if } q = 1 \Rightarrow \text{no vehicles behind} \\ d_{0, \beta_{q-1}} + d_{0, \beta_q} * t_{HW, \beta_{q-1}} + \\ 0.5 * (TW_{\beta_q} + TW_{\beta_{q-1}}), & \text{otherwise} \end{cases} \quad (3.4)$$

$$\{ \beta_q \in \text{All neighbors} : n_{Lane, \beta_q} \neq n_{Lane, E} \}$$

The initial longitudinal position of the neighbor vehicle on the inertial reference frame, x_{0, β_q} , is calculated from d_{0, β_q} as shown in equation 3.5.

$$x_{0, \beta_q} = r_{road} * \sin \frac{d_{0, \beta_q}}{r_{road}} \quad (3.5)$$

$$\{ \beta_q \in \text{All neighbors} : n_{Lane, \beta_q} \neq n_{Lane, E} \}$$

3.3.5. Maximum permissible lateral drift due to KLE

The maximum lateral distance that the host vehicle can travel due to the KLE before reaching the edge of the road, where road edge hazards such as guardrails, trees/poles, pedestrians, etc, exist, is denoted as the maximum permissible lateral drift, DTE . Depending on the direction and magnitude of the KLE drift radius and the curvature of the road, the DTE can either be the distance from the host vehicle to the leftmost road edge or to the rightmost road edge.

The resulting drift direction in a scenario arising from different combinations of road curvature and drift curvature is explained in table 3.1. This is determined mathematically as given in equation 3.6, where $drift_{side}$ is positive when the resultant drift is towards the left side of

Case	KLE curve	Road curve	Radius comparison	Resultant drift
Case 1	To right	To right	$ r_{KLE} < r_{road} $	To right
Case 2	To right	To right	$ r_{KLE} > r_{road} $	To left
Case 3	To right	To left	Either way	To right
Case 4	To left	To left	$ r_{KLE} < r_{road} $	To left
Case 5	To left	To left	$ r_{KLE} > r_{road} $	To right
Case 6	To left	To right	Either way	To left

Table 3.1.: The resultant drift direction due to road and KLE curvature

the road and negative when the resultant drift is towards the right.

$$drift_{side} = \begin{cases} 1 * \text{signum}(r_{KLE}), & \text{if } \text{signum}(r_{KLE}) \neq \text{signum}(r_{road}) \\ 1 * \text{signum}(r_{KLE}) * \text{signum}(|r_{road}| - |r_{KLE}|), & \text{otherwise} \end{cases} \quad (3.6)$$

The lateral distance between the host vehicle and the leftmost edge of the road in the scenario, DTE_{left} , is determined using equation 3.7.

$$DTE_{left} = (n_{Lanes} - n_{Lane, E} + 0.5) * W_L - 0.5 * TW_E - CO_E \\ + (n_{Lanes} - n_{Lane, E} + 1) * W_{LM} + LTR_{right} \quad (3.7)$$

And the lateral distance from the host vehicle to the rightmost edge of the road, DTE_{right} , is given by the equation 3.8.

$$DTE_{right} = (n_{Lane, E} - 0.5) * W_L - 0.5 * TW_E + CO_E \\ + (n_{Lane, E}) * W_{LM} + LTR_{left} \quad (3.8)$$

DTE for a given traffic scenario is dependent on the resultant drift direction of the host vehicle and it is expressed as shown in equation 3.9.

$$DTE = \begin{cases} DTE_{right} & \text{if } drift_{side} < 0 \\ DTE_{left} & \text{if } drift_{side} > 0 \end{cases} \quad (3.9)$$

In order to calculate the time taken for the host vehicle to cover the lateral drift, $t_{C,Ed}$, the intersection of the paths taken by the host vehicle with the road edge curve must be deter-

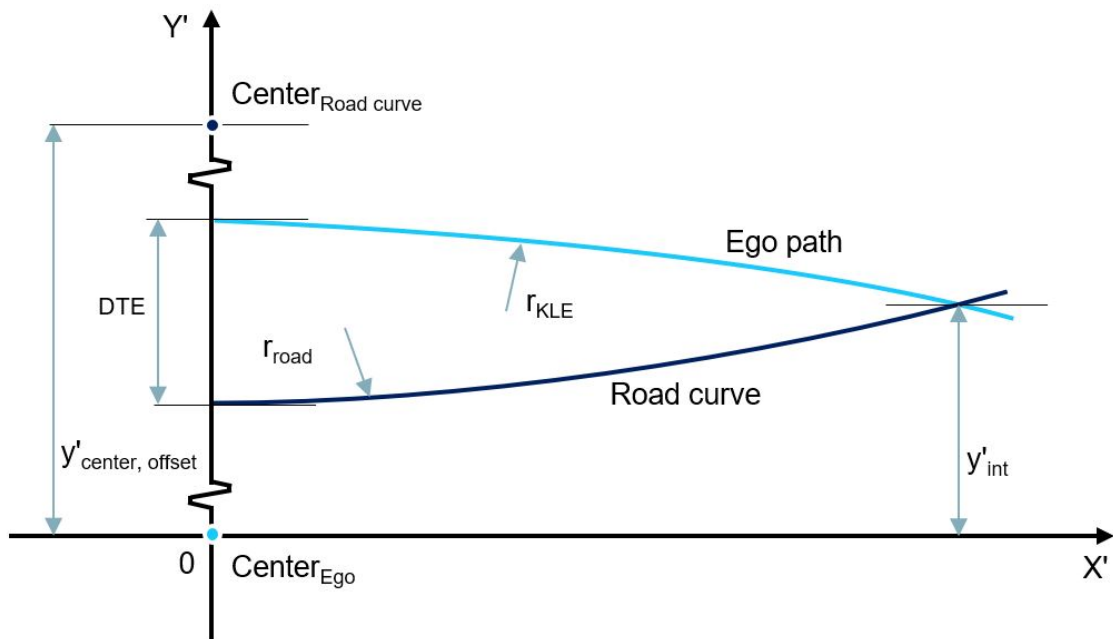


Figure 3.6.: Intersection of the host vehicle's path with the road curvature

mined. This intersection is visualized in figure 3.6, where the curvature of the host vehicle, *Ego path*, and the curvature of the road, *Road curve*, are illustrated in a shifted co-ordinate frame, X'-Y'. In this frame, the center of the circle representing the host vehicle's path lies at the origin, and the radius of the curve is positive for a left turn and negative for a right turn.

To calculate the intersection of the two curves, the distance between the centers of the two curves, denoted as $y'_{center,offset}$, is important. It is determined using equation 3.10. The initial vertical distance between the two curves is the maximum permissible lateral drift, *DTE*, refer to equation 3.9.

$$y'_{center,offset} = r_{road} - r_{KLE} + DTE * drift_{side} \quad (3.10)$$

The equation of the two circles is given in 3.11, where x' & y' are the X & Y co-ordinates along the curves in X'-Y' frame.

$$\begin{aligned} x'^2 + y'^2 &= r_{KLE}^2 \\ x'^2 + (y' - y'_{center,offset})^2 &= r_{road}^2 \end{aligned} \quad (3.11)$$

The intersection of the two circles is given by equation 3.12, where y'_{int} is the point of intersection of the two curves on the Y-axis.

$$y'_{int} = (y'_{center,offset} + \frac{r_{KLE}^2 - r_{road}^2}{2y'_{center,offset}}) * 0.5 \quad (3.12)$$

Finally $t_{C,Ed}$ is calculated using equation 3.13, where $v_{0,E}$ is the initial velocity of the host vehicle.

$$t_{C,Ed} = \cos^{-1} \left(\frac{|y'_{int}|}{|r_{KLE}|} \right) * \frac{|r_{KLE}|}{v_{0,E}} \quad (3.13)$$

3.3.6. Trajectory tracking

The trajectories of all the vehicles are determined by the traffic model to get their exact position throughout the simulation for any particular scenario. The model calculates the vehicle's center at every instant of the simulation, in δt increment, depending on the velocity, v , and the curvature of the designated path of the corresponding vehicle, r . Based on the dimension and orientation of the vehicles, the traffic model can calculate the co-ordinates of all the vehicle corners from the co-ordinates of its center.

In any given scenario, the host vehicle follows a designated path denoted as r_{KLE} , while the other vehicles follow the path of the road, represented by r_{road} . Therefore, at any given instant, t , the total distance traveled by the vehicle from its initial position along its respective path, denoted by $d(t)$, can be determined as given in equation 3.14. It relies on the velocity of the vehicle at every instant of the simulation from the beginning of the simulation up until the instant t .

$$d(t) = \sum_{T=1}^t v(T) * \delta t \quad (3.14)$$

The corresponding angle of orientation of the vehicle with respect to the inertial reference frame X-Y, denoted as $\phi(t)$, is obtained from $d(t)$ using equation 3.15.

$$\phi(t) = \sin^{-1}\left(\frac{d(t)}{r}\right) \quad (3.15)$$

As multiple vehicles are present in the simulation, the trajectories don't always begin from the origin of the X-Y frame. Thus, equation 3.16 includes the impact of the initial X co-ordinate, x_0 , on $\phi(t)$. And equation 3.17 includes the effects of the initial Y co-ordinate, y_0 , on $\phi(t)$.

$$\begin{aligned} \phi_0 &= \sin^{-1}\left(\frac{x_0}{r}\right) \\ \phi(t) &= \phi(t) + \phi_0 \end{aligned} \quad (3.16)$$

The exact X and Y co-ordinates of the vehicle center at an instant t is calculated as shown in equation 3.17 and it is illustrated in figure 3.7.

$$\begin{aligned} x_{center}(t) &= r * \sin\phi(t) \\ y_{center}(t) &= r * (1 - \cos\phi(t)) + y_0 \end{aligned} \quad (3.17)$$

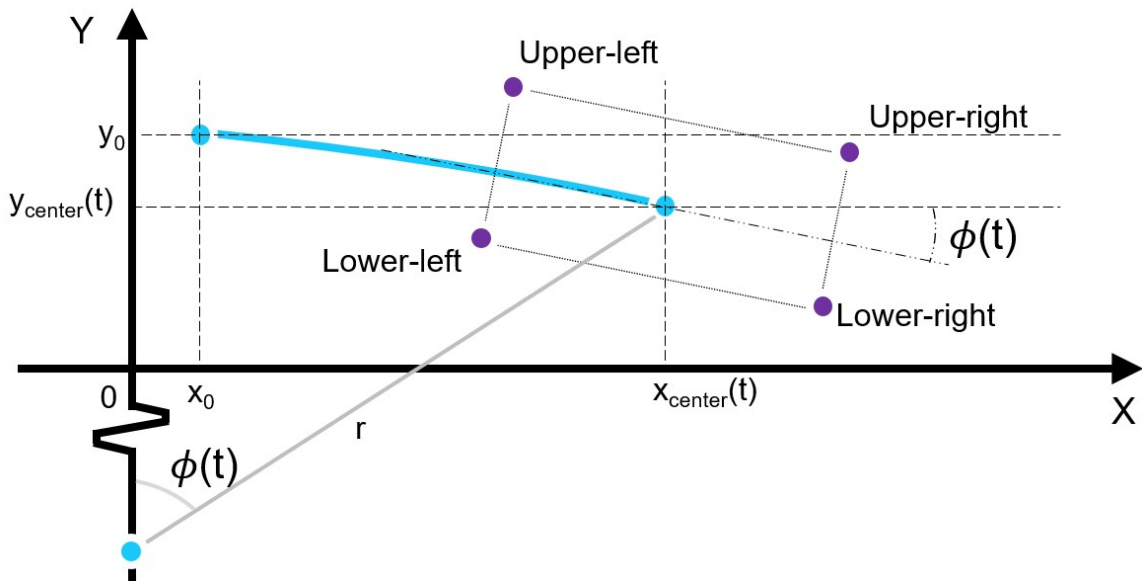


Figure 3.7.: Trajectory of vehicle center

The X and Y co-ordinates of the vehicle center, as given in equation 3.17, are used to project the vehicle as a rectangle using equation 3.18. The four corners of the rectangles upper left, upper right, lower right, and lower left are denoted as UL , UR , LR , and LL respectively. The rotation of the rectangle (vehicle) follows a clockwise direction for a curve with a negative radius (right turn) and vice versa. Geometrically, it can be inferred that the magnitude of rotation of the rectangle is equal to the magnitude of the angle at the center of the curve for any point along it, but with opposite signs. Therefore, the negative value of $\phi(t)$ is used as

the angle of rotation of the rectangle in equation 3.18.

$$\begin{aligned}
 x_{UL}(t) &= x_{center}(t) - \cos(-\phi(t)) * (WB)/2 + \sin(-\phi(t)) * (TW)/2 \\
 y_{UL}(t) &= y_{center}(t) + \sin(-\phi(t)) * (WB)/2 + \cos(-\phi(t)) * (TW)/2 \\
 x_{UR}(t) &= x_{center}(t) + \cos(-\phi(t)) * (WB)/2 + \sin(-\phi(t)) * (TW)/2 \\
 y_{UR}(t) &= y_{center}(t) - \sin(-\phi(t)) * (WB)/2 + \cos(-\phi(t)) * (TW)/2 \\
 x_{LL}(t) &= x_{center}(t) - \cos(-\phi(t)) * (WB)/2 - \sin(-\phi(t)) * (TW)/2 \\
 y_{LL}(t) &= y_{center}(t) + \sin(-\phi(t)) * (WB)/2 - \cos(-\phi(t)) * (TW)/2 \\
 x_{LR}(t) &= x_{center}(t) + \cos(-\phi(t)) * (WB)/2 - \sin(-\phi(t)) * (TW)/2 \\
 y_{LR}(t) &= y_{center}(t) - \sin(-\phi(t)) * (WB)/2 - \cos(-\phi(t)) * (TW)/2
 \end{aligned} \tag{3.18}$$

3.3.7. Collision detection

After calculating the trajectories of the vehicles, the next step is to determine whether a collision occurred between the host vehicle and the neighboring vehicles during the simulation. The vehicles are represented as rectangles throughout the simulation, and their corresponding X and Y co-ordinates are available at each instant. Therefore, when two rectangles representing the two vehicles intersect with one another it indicates that a collision occurred in the simulation. There are few built-in MATLAB functions that can detect the intersection of two rectangles. The first function is "rectint", which determines if two non-rotated rectangles are intersecting. However, this function can not handle rotated rectangles. The second function is "intersect", which converts the rectangles into polygons and calculates the area of overlap between the polygons. Nevertheless, this approach is computationally very expensive. In order to overcome the limitations of these functions, an adaptation of the separating axis theorem is employed in the proposed model to detect intersections between two rectangles. This method offers an efficient solution for collision detection in the simulation.

The Separating Axis Theorem states that two non-convex-shaped objects are separate if there exists a straight line that can separate the two objects. When applying the separating axis theorem to identify the intersection between two polygons, both together having 'm' edges in total, all the corners of the polygons are projected onto the 'm' principal axes. The principal axes are parallel to the edges of the polygons. According to the theorem, the two objects intersect only when the projected edges overlap on all of the principal axes. In other words, if there exists a principal axis where the projected corners do not overlap, it can be mathematically proven that there exists a straight line that can separate the two polygons. Therefore, by analyzing the overlap of the projected corners on the principal axes, the separating axis theorem can be used to determine whether or not two polygons intersect.

When adopting this theorem to the intersection of two rectangles, the number of unique (non-parallel) principal axes reduces to four, $PA1 - PA4$. As the opposite edges of a rectangle

are parallel to each other. The separating axis theorem is depicted for two rotated rectangles, A & B, in figure 3.8. Where the projected corners of these two rectangles overlap on all four principal axes. Principal axes are anchored from the origin, and the X & Y co-ordinates of a point on each of the principal axes at a given instant of the simulation are calculated by using equation 3.19.

$$\begin{aligned}
 x_{PA1}(t) &= x_{A, UR}(t) - x_{A, UL}(t) & \& \quad y_{PA1}(t) &= y_{A, UR}(t) - y_{A, UL}(t) \\
 x_{PA2}(t) &= x_{A, UR}(t) - x_{A, LR}(t) & \& \quad y_{PA2}(t) &= y_{A, UR}(t) - y_{A, LR}(t) \\
 x_{PA3}(t) &= x_{B, UR}(t) - x_{B, UL}(t) & \& \quad y_{PA3}(t) &= y_{B, UR}(t) - y_{B, UL}(t) \\
 x_{PA4}(t) &= x_{B, UR}(t) - x_{B, LR}(t) & \& \quad y_{PA4}(t) &= y_{B, UR}(t) - y_{B, LR}(t)
 \end{aligned} \tag{3.19}$$

The projection of all corners, $\forall k$, of both the rectangles, $\forall j$, onto all of the four principal axes, $\forall i$, is determined using equation 3.20.

$$PAi_{j, k}(t) = \frac{x_{j, k}(t) * x_{PAi}(t) + y_{j, k}(t) * y_{PAi}(t)}{x_{PAi}(t)^2 + y_{PAi}(t)^2} \tag{3.20}$$

$\{ i \in \text{All principal axes, } j \in \text{All rectangles, } k \in \text{All corners} \}$

The corresponding minimum and maximum value of the projected corners for both rectangles, $\forall k$, onto each of the four principal axes, $\forall i$, are given by equation 3.21.

$$\begin{aligned}
 PAi_{j, min}(t) &= \min (PAi_{j, k}(t) , \forall k) \\
 PAi_{j, max}(t) &= \max (PAi_{j, k}(t) , \forall k)
 \end{aligned} \tag{3.21}$$

The overlap of the projected corners on a particular principal axis is determined mathematically for every instant of the simulation using equation 3.22. The two rectangles intersect only if the projected corners overlap on all four principal axes, as illustrated in figure 3.8(a) - 3.8(d).

$$Intersect = True, \text{ if } \forall i \begin{cases} PAi_A, min(t) \leq PAi_B, min(t) \leq PAi_A, max(t), \text{ or} \\ PAi_B, min(t) \leq PAi_A, min(t) \leq PAi_B, max(t) \end{cases} \tag{3.22}$$

The collision of the host vehicle and each neighboring vehicle is checked individually at every instant of the simulation, from the beginning until either t_{KLE} , or $t_{C,Ed}$, whichever occurs earlier. The first instant at which the rectangles representing the host vehicle and the neighbor vehicle β_q intersect with each other is denoted by t_{C,β_q} . In case multiple collisions between the host vehicle and different neighbor vehicles are detected, the very first collision between the host vehicle and the neighbors is denoted by $t_{C,\beta}$. It is the minimum of all t_{C,β_q} from all neighbors, i.e, $\forall \beta$. The simulation results in a collision, when either $t_{C,\beta}$ or $t_{C,Ed}$ or both are less than t_{KLE} . The colliding object of a collision is determined based on which collision occurs first. If $t_{C,\beta}$ is lower than $t_{C,Ed}$ then the colliding object is the neighbor vehicle; otherwise, the host vehicle leaves the road and collides with the road edge hazards such as

guardrail, tree, etc. The time of collision denoted as t_C , is determined using equation 3.23.

$$t_C = \begin{cases} t_{C,\beta}, & \text{if } t_{C,\beta} \leq t_{C,Ed} \ \& \ t_{C,\beta} \leq t_{KLE} \\ t_{C,Ed}, & \text{if } t_{C,Ed} \leq t_{C,\beta} \ \& \ t_{C,Ed} \leq t_{KLE} \\ n/a, & \text{otherwise} \end{cases} \quad (3.23)$$

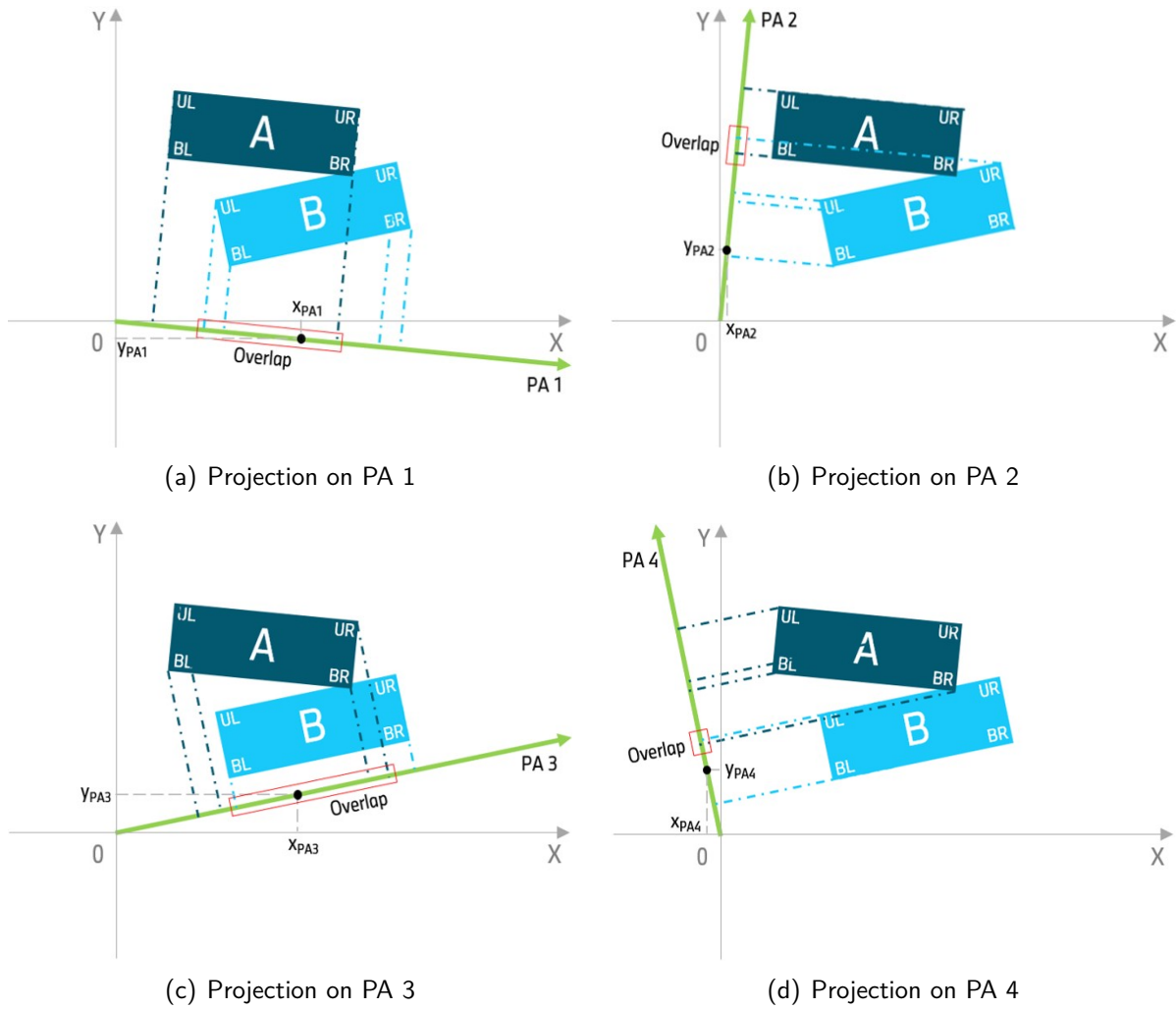


Figure 3.8.: *Illustration of separating axis theorem*

3.3.8. Traffic participants' controllability

3.3.8.1. Braking intervention of the road users

To simulate the dynamic interactions between the vehicles, the interventions of the vehicles in the form of braking are incorporated into the traffic model. The host vehicle brakes due to the ASC function, while the neighbor vehicle brakes in response to the perception of an imminent collision or danger, in the form of anticipatory braking. The braking intervention of the host and neighbor vehicle is indirectly dependent on one other. In order to model the realistic braking behavior, it is assumed, without contradiction, that the braking decision of

a driver or a system is not influenced by the anticipated behavior of the other vehicles, but rather relies primarily on the dynamic relative distances and relative velocities between the two vehicles. Therefore, in the proposed model, the braking interventions are validated simultaneously for both the host vehicle and the neighboring vehicle, aiming to establish a coherent braking behavior that closely resembles real-world scenarios.

Thus, in the proposed traffic model the braking behavior is modelled to have a reduction in the velocity at a constant rate of d_{Brk} , assuming a constant deceleration rate of -4 m/s^2 . The braking intervention conditions described in sections 3.3.8.3 and 3.3.8.4 are continuously monitored throughout the simulation. If the braking requirements are met at instant t_B , the corresponding braking intervention is implemented by reducing the vehicle's velocity, as shown in equation 3.24. The time difference between two instances monitored in the simulation is denoted as δt .

$$v_{\$}(t_B + \delta t) = v_{\$}(t_B) - d_{Brk} * \delta t \quad (3.24)$$

{ $\$ \in$ All vehicles meeting braking conditions }

As multiple road users are involved in a scenario, it is necessary to determine the need for braking intervention for each of the traffic participants. In this proposed methodology, although parallel braking interventions from both the neighbor vehicle and host vehicle are considered, the interventions are checked one neighbor at a time with the host vehicle. Since each neighbor is initialized to a random starting position based on the input data, it is important to ensure a chronological sequence of interventions by the road users. Therefore, if interventions from the host vehicle are deemed necessary for more than one neighbor, a re-evaluation of the braking interventions is required to maintain the chronological correctness of the host vehicle's braking. This re-evaluation process is carried out in ascending order for each of the neighbors, starting with the neighbor having the earliest initial intervention time of the host vehicle, and concluding with the neighbor that has the latest initial intervention time of the host vehicle.

3.3.8.2. Relative positioning between the vehicles

The relative positioning and orientation of the vehicles in the traffic model along with corresponding parameters that define the same are depicted in figure 3.9. It is illustrating a traffic scenario, where the host vehicle is intruding onto the neighboring lane at instant t and the host vehicle is slightly but not completely ahead of the neighbor vehicle β . The attributes of host and neighbor vehicles are denoted by the subscripts E & β respectively.

Distance between the vehicles is necessary to judge the need for braking. It is determined based on the co-ordinates of the vehicle center, and the corresponding maximum distance from the center of the vehicle to both the inner and the outer corners of the vehicle along the X & Y axes which are represented as $x_{ctc,min}(t)$, $x_{ctc,max}(t)$, $y_{ctc,min}(t)$ & $y_{ctc,max}(t)$ respectively, refer equation 3.25.

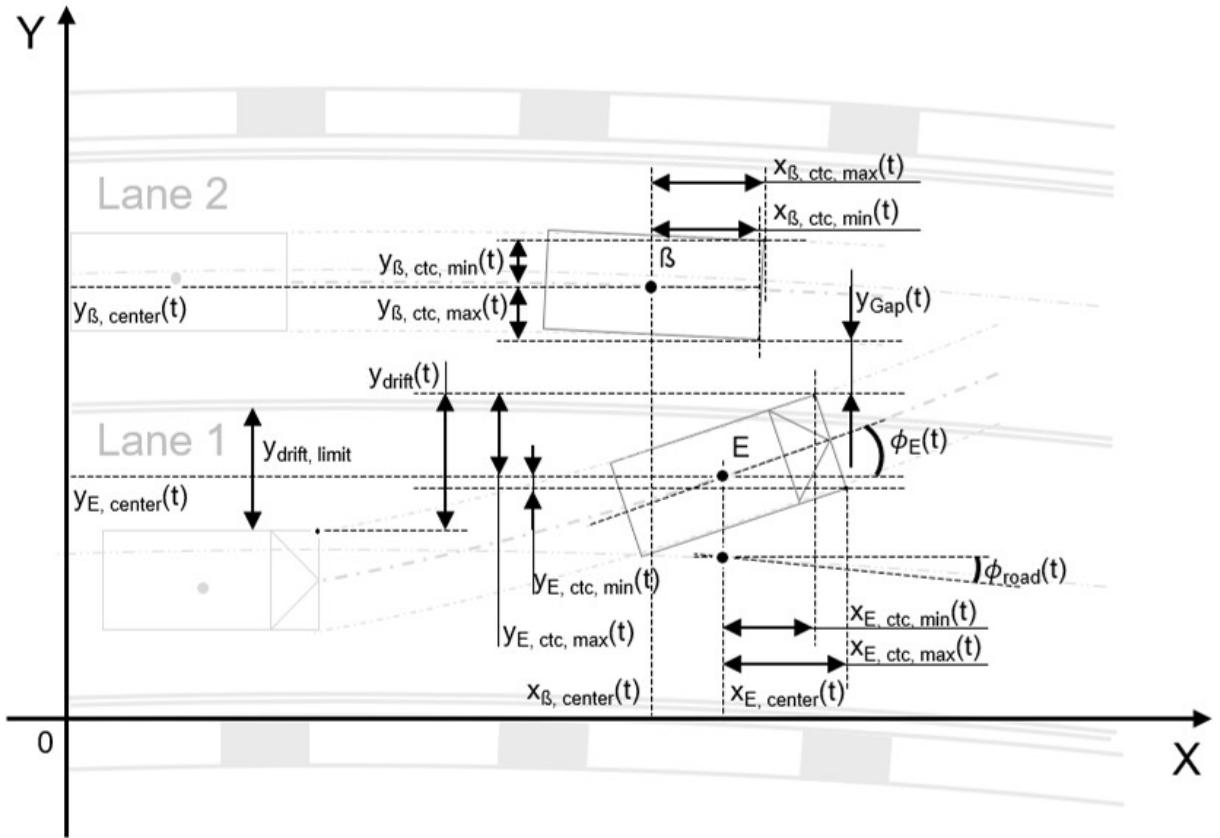


Figure 3.9.: Relative distances between the vehicles

$$\begin{aligned}
 x_{ctc,min}(t) &= 0.5 * WB * \cos |\phi(t)| - 0.5 * TW * \sin |\phi(t)| \\
 x_{ctc,max}(t) &= 0.5 * WB * \cos |\phi(t)| + 0.5 * TW * \sin |\phi(t)| \\
 y_{ctc,min}(t) &= 0.5 * TW * \cos |\phi(t)| - 0.5 * WB * \sin |\phi(t)| \\
 y_{ctc,max}(t) &= 0.5 * TW * \cos |\phi(t)| + 0.5 * WB * \sin |\phi(t)|
 \end{aligned} \tag{3.25}$$

Additionally, to judge the braking necessity, it is also important to determine the relative velocity and acceleration between the host vehicle and the neighbor vehicle along the longitudinal (X-axis) and lateral (Y-axis) directions given by $v_{r, x}(t)$, $v_{r, y}(t)$, $a_{r, x}(t)$, and $a_{r, y}(t)$ respectively, refer equation 3.26 & 3.27.

$$\begin{aligned}
 v_{r, x}(t) &= |v_E(t) * \cos\phi_E(t) - v_\beta(t) * \cos\phi_E(t)| \\
 v_{r, y}(t) &= |v_E(t) * \sin\phi_E(t) - v_\beta(t) * \sin\phi_\beta(t)|
 \end{aligned} \tag{3.26}$$

$$\begin{aligned}
 a_{r, x}(t) &= \left| \frac{v_E(t)^2 * \sin\phi_E(t)}{r_{KLE}} - \frac{v_\beta(t)^2 * \sin\phi_\beta(t)}{r_{road}} \right| \\
 a_{r, y}(t) &= \left| \frac{v_E(t)^2 * \cos\phi_E(t)}{r_{KLE}} - \frac{v_\beta(t)^2 * \cos\phi_\beta(t)}{r_{road}} \right|
 \end{aligned} \tag{3.27}$$

As the measurements in the traffic model are based on the X-Y frame, an additional parameter $\phi_{road}(t)$ is necessary to determine the orientation of the host vehicle relative to the curvature of the road. $\phi_{road}(t)$ represents the expected angular orientation of the host vehicle due to

the road curvature for the corresponding longitudinal position of the host vehicle relative to the X-Y frame. This parameter is determined under the assumption that the host vehicle does not have any lane-keeping failure, as shown in equation 3.28.

$$\phi_{road}(t) = \sin^{-1}\left(\frac{x_{E, center}(t)}{r_{road}}\right) \quad (3.28)$$

3.3.8.3. Avoid Side Collision

ASC is one of the inbuilt safety functionality assumed for the L3 Function that is incorporated in the simulation model. Its purpose is to brake the host vehicle, in order to mitigate and/or prevent lateral collision of the host vehicle with another vehicle. It is assumed, without contradiction, that the ASC doesn't activate for imminent collisions with road edge hazards. The ASC functionality is activated only when all of the following requirements are satisfied.

- *First requirement:* A neighboring vehicle must exist within a range of 3m to the front and 3m to the rear of the host vehicle. This requirement is satisfied when the X coordinate of at least one of the neighbor corners lies within the upper and lower limit of $x_{E, BB}(t)$, which are the limits of a bounding box representing a 3m range to the front and rear of the host vehicle as given in equation 3.29. And $x_{BB}(t)$ is the maximum distance along the X-axis between the vehicle center and a point 3m away from the outer corner of the host vehicle.

$$\begin{aligned} x_{BB}(t) &= x_{E, ctc,max}(t) + 3 \\ x_{E, BB}(t) &= x_{E, center}(t) \pm x_{BB}(t) \end{aligned} \quad (3.29)$$

- *Second requirement:* The lateral gap between the host vehicle and the neighbor vehicle, denoted as $y_{Gap}(t)$, must be less than the minimum safe lateral gap, which is assumed as 0.6m for the purpose of this study. This requirement is satisfied if $y_{Gap}(t) \leq 0.6m$. The lateral gap between the host vehicle and the neighbor vehicle is determined using equation 3.30.

$$y_{Gap}(t) = |y_{E, center}(t) - y_{\beta, center}(t)| - y_{\beta, ctc,max}(t) - y_{E, ctc,max}(t) \quad (3.30)$$

- *Third requirement:* The relative velocity of the neighbor vehicle with respect to the host vehicle must be within ± 10 kmph. This requirement is satisfied when $|v_E(t) - v_{\beta}(t)| \leq 10$.
- *Fourth requirement:* The host vehicle is unable to overtake or maintain a lead over the neighbor vehicle without colliding with it, assuming that both vehicles continue driving further without altering their respective velocities. Due to the complexity of this requirement, it is construed as a series of three logical statements. Each statement describes a scenario where the host vehicle can safely surpass or maintain its lead over

the neighbor vehicle. Therefore, in order for the fourth requirement to be satisfied, all of the following statements must be false.

- *First statement:* The host vehicle is faster than the neighbor vehicle, and the host vehicle must be completely ahead. This statement is true when $v_E(t) \geq v_\beta(t)$ and $x_{E,R-N,F}(t) > 0$. Where $x_{E,R-N,F}(t)$ is the distance from the front of the neighbor vehicle to the rear of the host vehicle along the X-axis, which is determined using equation 3.31.

$$x_{E,R-N,F}(t) = (x_{E, center}(t) - x_{E, ctc,max}(t)) - (x_{\beta, center}(t) + x_{\beta, ctc,max}(t)) \quad (3.31)$$

- *Second statement:* The host vehicle is slower than the neighbor, and the host vehicle is fully behind the neighbor. This statement is true when $v_E(t) \leq v_\beta(t)$ and $x_{N,R-E,F}(t) > 0$. Where $x_{N,R-E,F}(t)$ is the distance from the front of the host vehicle to the rear of the neighbor vehicle along the X-axis, given by equation 3.32.

$$x_{N,R-E,F}(t) = (x_{\beta, center}(t) - x_{\beta, ctc,max}(t)) - (x_{E, center}(t) + x_{E, ctc,max}(t)) \quad (3.32)$$

- *Third statement:* The host vehicle is not completely ahead of the neighbor, but the host vehicle can safely overtake the neighbor vehicle. This statement is true when $x_{E,R-N,F}(t) < 0$ and $t_{y, gap} > t_{x, ER-NF}$. Where $t_{y, gap}$ is the time taken by the host vehicle to cover the lateral gap, $y_{Gap}(t)$, and it is calculated as shown in equation 3.33.

$$y_{Gap}(t) = v_{r, y}(t) * t_{y, gap} + 0.5 * a_{r, y}(t) * t_{y, gap}^2$$

$$\Rightarrow t_{y, gap} = \frac{-2 * v_{r, y}(t) + \sqrt{4 * v_{r, y}(t)^2 + 8 * a_{r, y}(t) * y_{Gap}(t)}}{2 * a_{r, y}(t)} \quad (3.33)$$

And $t_{x, ER-NF}$ is the time taken by the host vehicle to get ahead of the neighbor, i.e., the cover the distance $|x_{E,R-N,F}(t)|$, and it is determined using equation 3.34.

$$|x_{E,R-N,F}(t)| = v_{r, x}(t) * t_{x, ER-NF} + 0.5 * a_{r, x}(t) * t_{x, ER-NF}^2$$

$$\Rightarrow t_{x, ER-NF} = \frac{-2 * v_{r, x}(t) + \sqrt{4 * v_{r, x}(t)^2 + 8 * a_{r, x}(t) * |x_{E,R-N,F}(t)|}}{2 * a_{r, x}(t)} \quad (3.34)$$

Once all the four requirements of the ASC function are satisfied, the host vehicle begins to decelerate at a constant rate. The braking continues as long as the velocity of the host vehicle is more than zero, and all the requirements are still satisfied. However, the necessity of the third requirement is exempted once the function is activated, because when the ASC function is activated the relative velocity of the colliding vehicle becomes irrelevant and the function

continues to decelerate the vehicle till the collision is prevented or at the least is mitigated.

3.3.8.4. Neighbor vehicle braking

In reality, drivers typically initiate braking with a certain latency upon perceiving an imminent collision and/or any danger. The braking behavior of the driver is dependent on their ability to perceive the danger and is also dependent on their ability to react to the perceived danger. For modelling the driver's behavior, a conservative assumption is made, suggesting that the driver is able to perceive danger upon a visible lane intrusion, particularly when the collision with the intruding vehicle is imminent. Mathematically, it can be interpreted that for the neighbor driver to perceive danger and initiate braking, the following three requirements need to be satisfied.

- *First requirement:* The host vehicle is within the visibility range of the neighbor driver. This requirement can be interpreted as logical statements, that the front of the host vehicle is ahead of the neighbor and also that the distance between the rear of the host vehicle to the front of the neighbor vehicle isn't further away than a time headway of 5s. This requirement is true, when $x_{E,F-N,F}(t) > 0$ and $x_{E,R-N,F}(t) < v_{\beta}(t) * 5s$. Where $x_{E,F-N,F}(t)$ is the distance from the front of the neighbor vehicle to the front of the host vehicle, and $x_{E,R-N,F}(t)$ is the distance from the front of the neighbor vehicle to the rear of the host vehicle along the X-axis. Equation 3.35 is used for calculating the distances which are essential to determine the visibility aspect.

$$\begin{aligned}
 x_{E,F-N,F}(t) &= (x_{E, center}(t) + x_{E, ctc,max}(t)) - (x_{\beta, center}(t) + x_{\beta, ctc,max}(t)) \\
 x_{E,R-N,F}(t) &= (x_{E, center}(t) - x_{E, ctc,max}(t)) - (x_{\beta, center}(t) + x_{\beta, ctc,max}(t))
 \end{aligned}
 \tag{3.35}$$

- *Second requirement:* The host vehicle should intrude onto the lane of the neighbor vehicle. The lane intrusion of the host vehicle is dependent on the resultant drift of the host and the corresponding orientation of the host vehicle with respect to the road curvature. The lane intrusion requirement is satisfied, when $y_{drift}(t) \geq y_{drift, limit}$, indicating that the host vehicle has finally drifted into the lane of the neighboring vehicle. Where $y_{drift}(t)$ is the lateral drift of the host vehicle with respect to the road curvature from the beginning of the simulation and it is given by equation 3.36.

$$\begin{aligned}
 y_{drift}(t) &= | (y_{E, center}(t) - y_{0, E}) - r_{road} * (1 - \cos\phi_{road}(t)) | - 0.5 * TW_E \\
 &\quad + 0.5 * TW_E * \cos\phi_E(t) + | 0.5 * WB_E * \sin\phi_E(t) |
 \end{aligned}
 \tag{3.36}$$

And $y_{drift, limit}$ is the lateral distance between the outer edge of the host vehicle until the lane of the neighbor vehicle as given in equation 3.37.

$$y_{drift, limit} = W_L + W_{LM} - TW_E - CO_E * drift_{side}
 \tag{3.37}$$

- *Third requirement:* The neighbor vehicle is set on a collision course with the host vehicle, which is visibly intruding onto the lane of the neighbor vehicle, assuming that both vehicles continue to drive without changing their respective velocities. There are only two possible situations that can lead the neighbor vehicle on a collision course and the third requirement is satisfied when either one of the two statements is true.
 - *First Statement:* The host vehicle is slower than the neighbor vehicle and it is fully ahead of the neighbor. This is true when $v_{\beta}(t) \geq v_E(t)$ and $x_{E,R-N,F}(t) > 0$, refer equation 3.31.
 - *Second Statement:* The host vehicle is not completely in front of the neighbor and the neighbor vehicle is unable to safely overtake the host vehicle. This statement is true when $x_{E,R-N,F}(t) < 0$, refer equation 3.31, $x_{N,R-E,F}(t) < 0$, refer equation 3.32, $x_{E,F-N,F}(t) > 0$, refer equation 3.35, and $t_{x, NR-EF} < t_{y, gap}$. Where $t_{x, NR-EF}$ is the time taken by the neighbor vehicle to get ahead of the host vehicle, refer equation 3.38, and $t_{y, gap}$ is the time taken for the host vehicle to cover the current lateral gap, refer equation 3.33.

$$\begin{aligned}
 |x_{N,R-E,F}(t)| &= v_{r, x}(t) * t_{x, NR-EF} + 0.5 * a_{r, x}(t) * t_{x, NR-EF}^2 \\
 \Rightarrow t_{x, NR-EF} &= \frac{-2 * v_{r, x}(t) + \sqrt{4 * v_{r, x}(t)^2 + 8 * a_{r, x}(t) * |x_{N,R-E,F}(t)|}}{2 * a_{r, x}(t)}
 \end{aligned}
 \tag{3.38}$$

For modelling the braking behavior of a driver the perception of the danger alone is not sufficient. In reality, there always exists a latency between the perception of danger and the counteraction, this is known as the driver brake reaction time, $t_{RT, \beta}$. The effect of brake reaction time is included as shown in equation 3.39. Where $t_{p0, \beta}$ is the first instant at which danger perception requirements are satisfied for the neighbor vehicle β .

$$t_{B, \beta} = \begin{cases} t_{p0, \beta} + t_{RT, \beta}, & \text{if } \forall t \in [t_{p0, \beta}, t_{B, \beta}] \text{ Danger perception} = \text{True} \\ n/a, & \text{otherwise} \end{cases}
 \tag{3.39}$$

In order to account for the latency, the neighbor vehicle starts to decelerate $t_{RT, \beta}$ seconds after $t_{p0, \beta}$, only if the danger perception requirements are met even during the latency, i.e., $t_{RT, \beta}$ seconds. Once the neighbor vehicle starts decelerating, i.e., at $t_{B, \beta}$, the neighbor continues to brake as long as its velocity is more than zero and all the danger perceptions requirements are still satisfied.

3.3.9. Classification of collision

The collisions of the host vehicle in the traffic model are broadly classified into two categories based on its colliding object, which is either a neighbor vehicle or a road edge hazard. For the collisions with neighbor vehicles, the different possible combinations of collision types for

the host vehicle and the neighbor vehicle are full frontal & rear, small overlap frontal & rear, side-swipe with a vehicle, and side-impact & front collisions. Collision types resulting from the collision of a host vehicle with road edge hazards are side-swipe with an obstacle, full frontal with an obstacle, small overlap frontal with an obstacle, and rollover collision. After a collision is detected by the model along with the colliding object as explained in section 3.3.7. The traffic model utilizes a sequential methodology to determine the collision type based on the colliding object, as described further in this section.

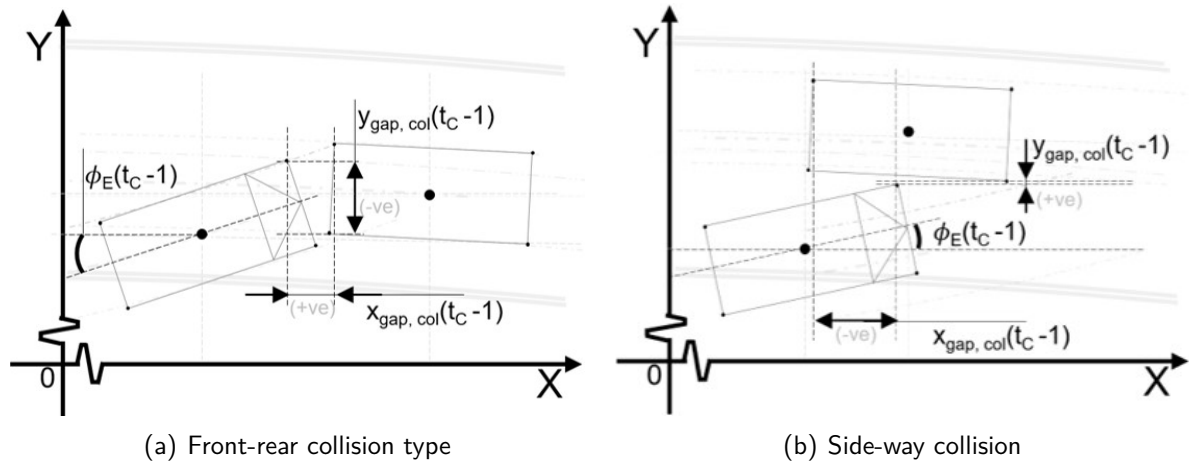


Figure 3.10.: Position and orientation of vehicles before collision

For collisions of the host vehicle with a neighbor vehicle, the model assesses whether the collision is a front-rear collision, where one vehicle is in a front-end collision and the other in a rear-end collision, or a side-way collision, as shown in figure 3.10(a) and 3.10(b) respectively. The collision types are identified by the model by checking sequentially if the conditions for each of the categories and sub-categories as listed below are getting satisfied.

- *Front-rear collision with neighbor:* At the instant just before the collision, $t_C - 1$, the vehicles will overlap one another either partially or completely in the lateral direction, i.e. along Y-axis, and will maintain a small gap between each other in the longitudinal direction, i.e. along X-axis, as depicted in figure 3.10(a). Mathematically, this geometric condition is satisfied when $x_{gap,col}(t_C - 1) > 0$, and $y_{gap,col}(t_C - 1) < 0$. Where $x_{gap,col}(t_C - 1)$ is the distance between the inner corners of the two vehicles measured along the X-axis using equation 3.40.

$$x_{gap,col}(t_C - 1) = |x_{E, center}(t_C - 1) - x_{\beta, center}(t_C - 1)| - x(t_C - 1)_{E, ctc,min} - x(t_C - 1)_{\beta, ctc,min} \quad (3.40)$$

And $y_{gap,col}(t_C - 1)$ is the distance between outer corners of the vehicles along the Y-axis, refer equation 3.41.

$$y_{gap,col}(t_C - 1) = |y_{E, center}(t_C - 1) - y_{\beta, center}(t_C - 1)| - y_{E, ctc,max}(t_C - 1) - y_{\beta, ctc,max}(t_C - 1) \quad (3.41)$$

Additionally in the front-rear collisions, the extent of the frontal overlap decides whether the vehicle experiencing frontal collision is in a full frontal or small overlap frontal.

- *Full frontal & rear collision*: The frontal overlap of the vehicles along the Y-axis is more than 25% of the minimum value of the track width of the two vehicles. This condition is true when $|y_{gap,col}(t_C - 1)| > 0.25 * \min(TW_E, TW_\beta)$.
- *Small overlap frontal & rear collision*: The frontal overlap is less than 25% of the vehicle track width, i.e, $|y_{gap,col}(t_C - 1)| \leq 0.25 * \min(TW_E, TW_\beta)$.
- *Side-way collision with neighbor*: Collisions of the host vehicle with a neighbor vehicle that aren't meeting the conditions of the front-rear collision type fall under this category. The side-way collisions of two vehicles are further classified based on the angle of collision between the host vehicle and the neighbor vehicle, $\phi_{Col}(t_C)$ given by equation 3.42.

$$\phi_{Col}(t_C) = \phi_E(t_C) - \phi_{road}(t_C) \quad (3.42)$$

- *Side-swipe vs car*: The angle of collision is less than 15° , this is true when $\phi_{Col}(t_C) < 15^\circ$.
- *Side impact & side impact*: The angle of collision is more than 15° and the distance between the front side of both vehicles is less than 110 cm, which is the average hood length of a car [41]. This is true when $\phi_{Col}(t_C) > 15^\circ$ and $|x_{E,F-N,F}(t_C - 1)| < 110 \text{ cm}$.
- *Frontal & side impact*: The angle of collision is more than 15° and the distance between the front side of both vehicles is more than 110 cm. This is true when $\phi_{Col}(t_C) > 15^\circ$ and $|x_{E,F-N,F}(t_C - 1)| \geq 110 \text{ cm}$.

For collisions with the road edge hazards, the collision type is dependent both on the edge hazards under consideration and the collision angle, $\phi_{Col}(t_C)$. The different types of road edge hazards are introduced in the injury estimation stage as a percentage factor based on the occurrence fraction of the individual edge hazards and their corresponding collision types.

3.3.10. Injury risk estimation

For each collision type, a specific IRF is derived using logistic regression on accident database data. Other than the type of collision, another important parameter for the IRF is the impact velocity of the accident.

The IRF for front-end, rear-end, and side-impact collisions, which are near side & far side, are adopted from [42]. They are derived from the logistic regression on Japanese accident data. The generic form of IRF for severe injury and above, IL2+, is given in equation 3.43, where IRP_{driver} is the injury probability for the driver, γ_n are the risk factors and c_n are their corresponding coefficient as listed in 3.2.

$$IRP_{driver} = \frac{1}{1 + \exp [- (\gamma_0 + \gamma_1 * c_1 + \gamma_2 * c_2 + \dots + \gamma_n * c_n)]} \quad (3.43)$$

Risk factors (γ_n)		Coefficients (c_n)
Intercept		-4.909
DeltaV (km/h)		0.095
Crash direction	Front	-0.051
	Rear	-
	Near side	1.187
	Far side	1.016
Age		0.571
Belt use	Yes = 1, No = 0	-1.826
Vehicle type		Passenger car
		-0.279

Table 3.2.: Risk factors and the corresponding coefficient for the IRF

Since delta-V isn't available for all accident cases in the police database an estimation of this parameter, ΔV_{Pseudo} , is derived using equation 3.44. It is based on the mass and velocity of the struck and striking vehicles in the event of a collision which are m_1 , m_2 , V_1 & V_2 respectively.

$$\Delta V_{Pseudo} = \frac{m_2}{m_1 + m_2} * (V_1 + V_2) \quad (3.44)$$

The estimated value of the parameter is then converted to real delta-V values using equation 3.43. The general risk prediction algorithm from [42] is modified to account for the effects of a small overlap front collision as well. It is assumed, without contraction, that the delta-V for small overlap is between full frontal and side-way collision.

$$\Delta V = \begin{cases} 0.7 * \Delta V_{Pseudo}, & \text{Full frontal collision} \\ 0.75 * \Delta V_{Pseudo}, & \text{Small overlap front collision} \\ 0.8 * \Delta V_{Pseudo}, & \text{Side-way collision} \\ 0.8 * \Delta V_{Pseudo}, & \text{Rear-end collision} \end{cases} \quad (3.45)$$

IRF from 3.43 addresses only IL2+ probability. However, in order to obtain the injury probabilities for other injury levels the injury risk curves are shifted by changing the delta-V as indicated in table 3.3. The curves are shifted such that the curve from [42] is superimposed onto the injury risk curves obtained by using logistic regression to fit the accident data from

Collision type	IL1+	IL3+
Small overlap front	DeltaV + 15	DeltaV - 28
Full front	DeltaV + 15	DeltaV - 33
Rear-end	DeltaV + 30	DeltaV - 30
Near side	DeltaV + 22	DeltaV - 27
Far side	DeltaV + 22	DeltaV - 27

Table 3.3.: Shift in deltaV for IL1+ and IL3+ IRFs

German In-Depth Accident Study (GIDAS) filtered specifically for collisions with IL1+ and IL3+ injuries.

IRF indicating the overall injury risk for collisions with pedestrians is given by equation 3.46, where the injury probability is dependent on the velocity at which the pedestrian is struck, v . The function is derived using logistic regression to fit the accident data from GIDAS, filtered specifically for pedestrian collisions.

$$IRF_{ped} = \frac{1}{1 + \exp[-(a + b * V)]} \quad (3.46)$$

The parameters of the pedestrian IRF for IL2+ & IL3+ are listed in table 3.4. For the IL1+, the risk probability is considered as 1, as at least mild injury is imminent during collisions with pedestrians.

IRF parameter	IL2+	IL3+
a	1.911387	5.93883298
b	-0.07877268	-0.07833647

Table 3.4.: Parameters of IRF for collision with pedestrians

The injury probabilities of one vehicle for different injury levels due to sideswipe collisions with another vehicle and with guardrails (road edge hazard) are obtained from the analysis of data from National Automotive Sampling System (NASS) [43]. The injury probabilities of a vehicle due to rollover collision is inferred from the results of [44]. The injury probability for collisions between car and motorbike is also filtered from GIDAS for velocities below 60 kmph. The compiled injury probabilities are listed in table 3.5, where the injury probabilities are not obtained from an IRF making them independent of delta-V and/or collision angle.

Injury level	Collisions			
	Sideswipe Vs		Rollover	Car Vs Motorbike
	Vehicle	Guardrail		
IL1+	5.50 %	4.0 %	76.10 %	100 %
IL2+	0.09 %	0.055 %	17.60 %	4.41 %
IL3+	0.01 %	0.014 %	9.60 %	0 %

Table 3.5.: Injury probabilities for different collisions

The simulation of the traffic model can result in a collision of the host vehicle either with a neighboring vehicle or with a road edge hazard. The combination of different types of collision between the participants in the collision will result in different injury probability functions. The possible combinations of collision type outcomes with all the participants are shown in table 3.6. The combination of collision types for collision scenarios of the host vehicle with either a car or a commercial vehicle belong to cases 2 – 12 . The collision angle for cases 2 – 6 is less than 15° and for cases 7 – 12 it's more than 15°. Similarly, for collision with road edge hazards, cases 13 & 14, the collision angle is less than 15° for case 13 and for case 14 it's more than 15°.

Collision case	Colliding participant	Collision type for	
		Host vehicle	Participant
Case 1	None	No Crash	No Crash
Case 2	Neighbor	Rear-end	Full frontal
Case 3	Neighbor	Rear-end	Small overlap front
Case 4	Neighbor	Full frontal	Rear-end
Case 5	Neighbor	Small overlap front	Rear-end
Case 6	Neighbor	Sideswipe vs car	Sideswipe vs car
Case 7	Neighbor	Full frontal	Far side
Case 8	Neighbor	Full frontal	Near side
Case 9	Neighbor	Far side	Full frontal
Case 10	Neighbor	Near side	Full frontal
Case 11	Neighbor	Far side	Near side
Case 12	Neighbor	Near side	Far side
Case 13	Edge hazard	Collision angle $\leq 15^\circ$	
Case 14	Edge hazard	Collision angle $> 15^\circ$	
Case 15	Motorbike	Car vs motorbike	

Table 3.6.: Possible collision outcome cases

The road edge hazards considered in the traffic model are - guardrails, guardrail ramps, trees/poles, break-down cars, and pedestrians. As the collision mechanism for each hazard is different, the injury probabilities of cases 13 & 14 must account for each of the hazards factored by the likelihood of the host vehicle encountering the particular hazard. The sub-categories for cases 13 & 14 are listed in table 3.7.

Collision case	Colliding participant	Collision type for	
		Host vehicle	Participant
Case 13	Edge hazard	Collision angle $\leq 15^\circ$	
Case 13a	Guardrail	Sideswipe vs guardrail	NA
Case 13b	Guardrail ramp	Rollover	NA
Case 13c	Trees/ poles	Full frontal	NA
Case 13d	Break-down car	Sideswipe vs car	Sideswipe vs car
		Full frontal	Rear-end
Case 13e	Pedestrian	Car vs pedestrian	
Case 14	Edge hazard	Collision angle $> 15^\circ$	
Case 14a	Guardrail	Full frontal	NA
Case 14b	Guardrail ramp	Rollover	NA
Case 14c	Trees/ poles	Full frontal	NA
Case 14d	Break-down car	Full frontal	Near side
		Full frontal	Rear-end
Case 14e	Pedestrian	Car vs pedestrian	

Table 3.7.: Sub-categories for collision with road edge hazards

The likelihood of a road edge hazard, as shown in equation 3.47, is the ratio of the distance traveled by the host vehicle with KLE to the average distance between two road hazards of the same type. The likelihood of each of the road edge hazards considered in this study is listed

in table 3.8, and this likelihood information is assumed and derived from BMW campaigns. As this information is BMW proprietary, the values are not accurately recorded in this thesis work. The sum of the likelihood of all edge hazards is considered as one. Therefore, the likelihood of the edge hazard as a guardrail is obtained by subtraction of the sum of all other edge likelihoods from one.

$$p_{\text{hazard},x} = d(t_C)_E / l_{\text{hazard}, x} \quad (3.47)$$

Road edge hazard	Distance between two occurrences (m), $l_{\text{hazard}, x}$
Guardrail ramps	4×10^5 m
Trees/ Poles	5×10^4 m
Break-down vehicles	2×10^5 m
Pedestrians	2×10^5 m

Table 3.8.: Road edge hazard occurrence rates

The IRF for frontal collisions with a road edge hazard is considered to be the same as given in equation 3.43. However, the velocity of the host vehicle at the time of collision is taken as delta-V. The two sub-cases for collision with a break-down car, i.e., two sub-cases of case 14d, are assumed to happen in even likelihood. The IRF for them is adopted from equation 3.43. However, ΔV_{pseudo} is taken as the velocity of the host vehicle for both the host vehicle and the break-down vehicle. Refer to equation 3.45 for calculating delta-V.

The injury probability of a vehicle must not only account for the injury from the driver [42], but also include the risks from the co-passenger as well, based on the probability of the co-passenger being occupied, which is denoted as $perc_{\text{copassenger}}$. The injury risk probability of a vehicle in a collision is given in equation 3.48. It is assumed, without contradiction, that the IRF of the driver and co-passenger is the same and that the likelihood of the co-passenger seat being occupied is 0.35 both for the host vehicle and the neighbor vehicles.

$$IRP_{\text{vehicle}} = IRP_{\text{driver}} + perc_{\text{copassenger}} * IRP_{\text{driver}} * (1 - IRP_{\text{driver}}) \quad (3.48)$$

To determine the injury risk probability of a collision, the injury risk probabilities from all the participants involved in the collision must be considered. Considering a particular scenario, n , where the host vehicle and the neighbor, E & β , are involved in a collision having two different collision types, a & b , for the respective vehicles. The overall injury risk probability from the collision between two vehicles is given by equation 3.49.

$$IRP_{\text{collision}}(n) = IRP_{E, a} + IRP_{\beta, b} - IRP_{E, a} * IRP_{\beta, b} \quad (3.49)$$

Collision probability is defined as the percentage of the scenario simulations which leads to a collision, given in equation 3.50. Where $n_S(v)$ is the total number of scenario simulations in

which v is the initial velocity of the host vehicle given there is a KLE, and $n_{S,C}(v)$ is the number of scenario simulations out of $n_S(v)$ scenarios that result in a collision.

$$p_{collision}(v) = n_{S,C}(v) / n_S(v) \quad (3.50)$$

Overall injury risk probability of the L3 Function per hour is given by $IR\tilde{P}_{/h}$, refer equation 3.51, where f_{KLE} is the frequency of occurrence of KLE per hour of driving in L3 Function which is the exposure rate, $p_{vel}(v)$ is the probability that the vehicle is driven at a particular velocity v on the highway, and $p_{collision}(v)$ is the probability of collision of the vehicle driven at a velocity of v in L3 Function given there is a KLE.

$$IR\tilde{P}_{/h} = \sum_{v=1}^{60} p_{collision}(v) * p_{vel}(v) * f_{KLE} * \frac{1}{n_S(v)} \left[\sum_{n(v)=1}^{n_S(v)} IRP_{collision}(n(v)) \right] \quad (3.51)$$

4. Data Sources

The primary data source for the parameters of the Highway traffic model proposed in this thesis work is from various campaigns and studies carried out by BMW AG, specifically related to German highway traffic conditions. The data collected is in compliance with the German data protection policy ensuring the privacy of the users. As data from the campaigns are BMW's proprietary properties, the distribution and likelihood trend of the traffic model parameters relevant to the scope of this thesis work is discussed without revealing any specific value in the following sections.

4.1. Ambient characteristics parameters

Ambient characteristics provide a very detailed description of the road infrastructure and the surrounding environment of the traffic scenario.

Road curvature

As the simulation is only for a few seconds, the scenarios of the straight roads are simulated to have a very large radius of curvature. The probability curve of the curvature of the road based on BMW campaigns, specific to German highway roads are as shown in figure 4.1.

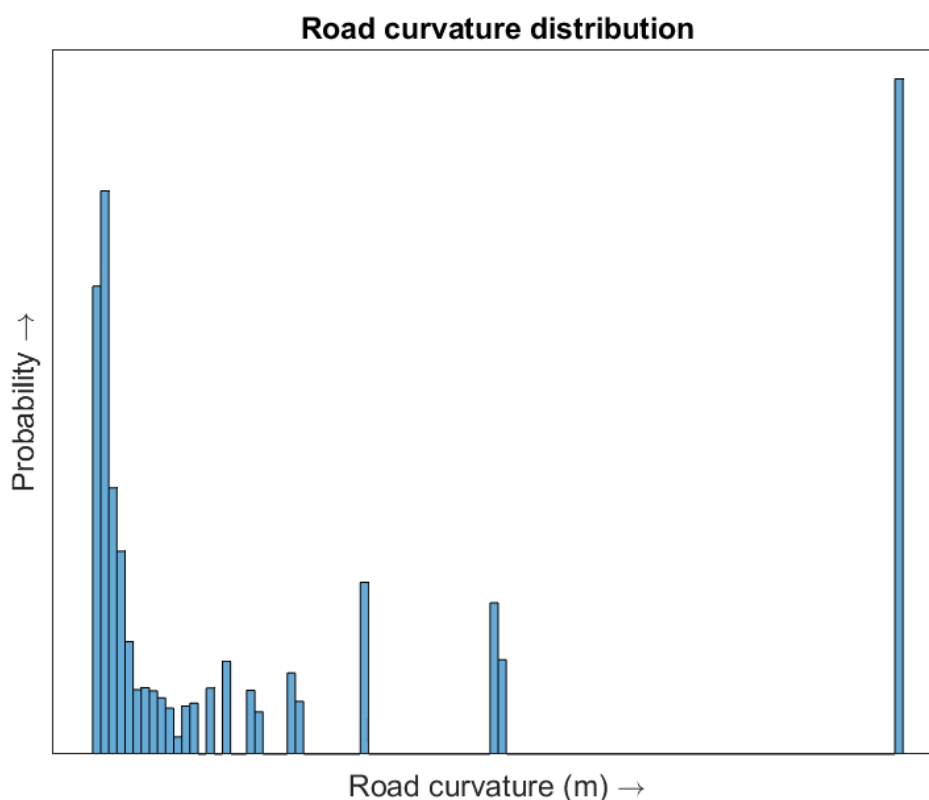


Figure 4.1.: Road curvature distribution

The road curvature parameter has both magnitude and sign, where the positive radius represents left turns and the negative represents right turns, and they are both sampled independently. The magnitude of the curvature is sampled from a multi-nominal distribution based on the likelihood as depicted in figure 4.1 and the sign is sampled from an equal chance bi-nominal distribution, refer table 4.1 for the sampling of the road curvature.

Road curvature, r_{road}	
$ r_{road} $	$signum(r_{road})$
$\sim \mathcal{M}_k(n; p_1, \dots, p_k)$	$\sim \mathcal{B}(n; 0.5)$

Table 4.1.: Sampling of road curvature

Number of lanes

The number of lanes for a scenario is sampled from a multi-nominal distribution as shown in equation 4.1. The likelihood of the number of lanes in a highway scenario, as listed in table 4.2, is an assumed distribution derived from the trends observed in BMW campaigns.

$$n_{Lanes} \sim \mathcal{M}_4(n; p_1, \dots, p_4) \quad (4.1)$$

Number of lanes, n_{Lanes}			
$n_{Lanes} = 1$	$n_{Lanes} = 2$	$n_{Lanes} = 3$	$n_{Lanes} = 4$
0 %	65 %	34 %	1 %

Table 4.2.: Likelihood of number of lanes in a scenario

Lane width

The lane width is sampled from a multi-nominal distribution as shown in equation 4.2. The likelihood of different lane width values, as indicated in table 4.3, is an assumed distribution derived from the trends observed in BMW campaigns.

$$W_L \sim \mathcal{M}_6(n; p_1, \dots, p_6) \quad (4.2)$$

Lane width in meters, W_L			
3.2 m	3.5 m	3.7 m	4.0 m
20 %	30 %	45 %	5 %

Table 4.3.: Likelihood lane width for a scenario

Lane markings width

The lane markings on the highway are not thin, as they need to be visible to the drivers on the road. Therefore, the width of the lane markings, W_{LM} , is an important parameter as they contribute to the total width of the road in an absolute mathematical sense. As per

the guidelines for road markings listed in [45], the lane markings width for German highway roads are 15 and/or 30 cm. Based on this the lane marking width is assumed, without any contraction, as 30 cm for all traffic scenarios.

Distance between lane edge and end of the road

Another important road parameter is the distance between the lane edge and the road edge, as this is essential to determine how far away are the road edge hazards from the lane edge. It is assumed, without any contradiction, that an emergency lane will be present next to the right-most lane in all scenarios and also that the distances between the lane and road edges are constant but varies only depending on the side of the road as shown in table 4.4.

According to the guidelines for designing motorways in Germany [46] lateral distance between the road edge and the lane edge can be extrapolated for the right-hand and left-hand side of the road as argued. Central reserves are recommended to have a width of 2.5m and this value is assumed as the lateral gap between the lane edge and the road edge on the right side. And for the left side, it is considered as 0.5m, because the recommended lateral safety space in the highway is 1m and a guard rail is assumed to be located exactly in the middle between the road and lane edges.

Distance between road edge and lane edge	
LTE_{left}	LTE_{right}
0.5 m	2.5 m

Table 4.4.: *Distance between the lane edge and road edge*

Driving mode

As the ODD of the assumed exemplary L3 Function includes both normal driving and emergency corridor maneuver, the driving mode is one of the most crucial ambient traffic parameters. The driving mode is solely dependent on the velocity of the host vehicle as shown in table 4.5 because the ODD of the exemplary L3 Function is divided based on the velocity.

Driving mode, D_{Mode}	
Emergency corridor - $D_{Mode, EC}$	Normal driving - $D_{Mode, ND}$
$1 \leq v_{0, E} < 30$ kmph	$30 \leq v_{0, E} \leq 60$ kmph

Table 4.5.: *Driving Mode*

Number of road users

Another important parameter that defines the surrounding environment is the number of road users in the scenario, q , and it is sampled at random based on discrete uniform distribution between 0 and the maximum number of road users other than the host vehicle, q_{max} , as indicated in equation 4.3. It is assumed, without contradiction, that the maximum number of

road users in the vicinity of the host vehicle is limited to five as the simulation of the KLE is only for a few seconds.

$$q \sim \mathcal{U} \{ 0, q_{max} \} \quad (4.3)$$

4.2. Ego characteristics parameters

Ego characteristics thoroughly describe the parameters to describe the initial position and the driving behavior of the host vehicle including its KLE behavior in the traffic model.

Vehicle centering error

The initial centering error of the host vehicle is sampled from a normal distribution as shown in equation 4.4. The sampling is based on the assumption, that the results from [47] are applicable to all highway traffic scenarios. According to this the deviation of the vehicle from the center line in a highway is less than 25 cm for most of the observations implying that the 6σ limit is within $\pm 25 \text{ cm}$.

$$C_{\$} \sim \mathcal{N} \left(0, \frac{0.25^2}{3} \right) \forall \$ \quad \{ \$ \in \text{All vehicles} \} \quad (4.4)$$

Lane assignment

The lane number is assigned to the host vehicle, $n_{Lane,E}$, at random based on a uniform discrete distribution between 1 and the number of lanes, n_{Lanes} , available in the given scenario. Refer to equation 4.5 for the sampling methodology.

$$n_{Lane,\$} \sim \mathcal{U} \{ 1, n_{Lanes} \} \forall \$ \quad \{ \$ \in \text{All vehicles} \} \quad (4.5)$$

Initial emergency lateral shift fraction

The initial emergency lateral shift fraction of the host vehicle, $frac_{shift,E}$, is the percentage of lateral offset of the vehicle necessary for the emergency corridor maneuver. And it is dependent on the initial velocity, v_0 of the vehicle, refer to equation 4.6. This is an assumed relation derived from the trends observed in BMW campaigns, specific to emergency corridor maneuvers in German highway scenarios.

$$frac_{shift,\$} = \begin{cases} 1, & \text{if } 1 \leq v_{0,\$} < 20 \text{ kmph} \\ 1 - \frac{4 * (v_{0,\$} - 20)}{100}, & \text{if } 20 \leq v_{0,\$} \leq 45 \text{ kmph} \end{cases}, \forall \$ \quad (4.6)$$

$$\{ \$ \in \text{All vehicles} \}$$

Initial longitudinal position

It is assumed, with any contradiction, that the initial longitudinal position of the host vehicle center is zero for the simulations, $x_{0,E} = 0$.

Initial velocity

The initial velocity of the host vehicle is a significant parameter that describes its driving behavior. All of the model input parameters are sampled for each discrete velocity of the host vehicle within the ODD, and multiple simulations are carried out for each velocity value. The probability with which the host vehicle is driving on the highway shown in figure 4.2, is an assumed distribution from trends observed in BMW campaigns. This is important for the determination of the overall injury probability.

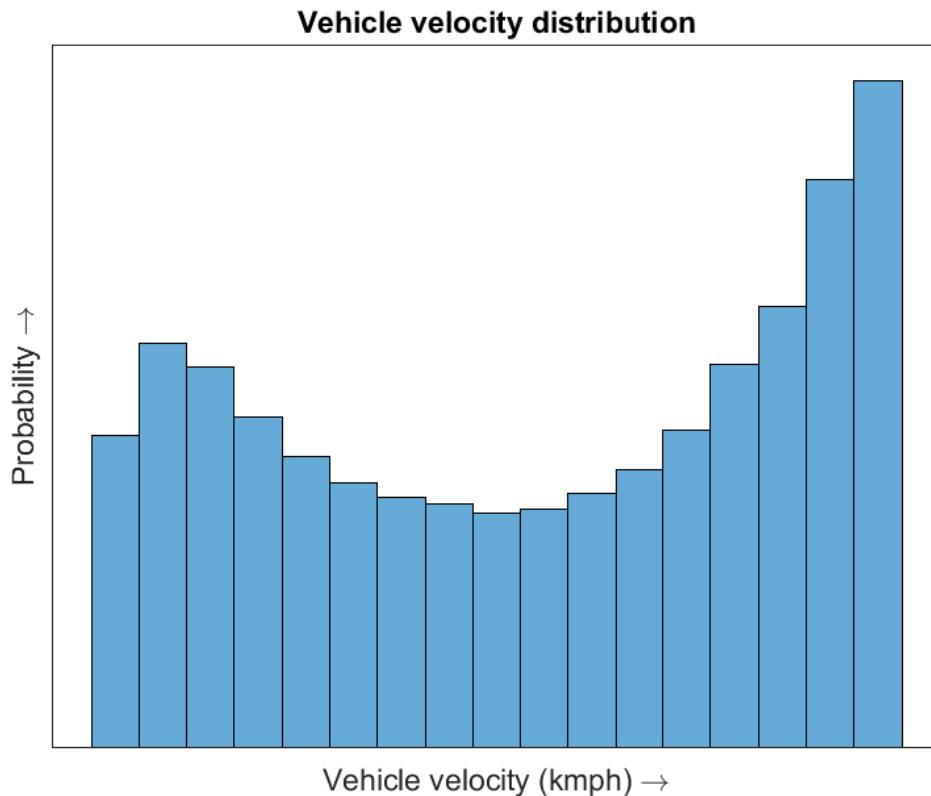


Figure 4.2.: Velocity distribution of the host vehicle

Keep Lane Error

As there is no data available with regards to the lane-keeping error the distribution function and limits are assumed in order to quantify the safety risk of L3 Function due to lane-keeping failure. The sampling of drift radius and duration of the KLE is shown in table 4.6.

KLE duration

The duration of KLE, t_{KLE} , is sampled directly from a uniform distribution where the upper limit is set based on the assumption that KLE will not occur for more than 5 seconds and the lower limit is set on the assumption that the KLE have a significant impact on the safety assessment only when it lasts more than 0.5 seconds.

KLE radius

The KLE drift radius comprises of both magnitude and sign where the magnitude of the radius is sampled from a uniform distribution, and the sign is sampled from an equal chance bi-nominal distribution. The range of the KLE drift radius magnitude is assumed, without contradiction, to be between 1000 to 5000 meters with respect to the X-Y frame.

KLE drift radius, r_{KLE}		KLE drift duration, t_{KLE}
$ r_{KLE} $	$signum(r_{KLE})$	
$\sim \mathcal{U}(1000, 5000)$	$\sim \mathcal{B}(n; 0.5)$	$\sim \mathcal{U}(0.5, 5)$

Table 4.6.: Sampling of KLE drift radius and drift duration

4.3. Neighbor characteristics parameters

Neighbor characteristics comprehensively describe the nature of the neighbor vehicles and their normal driving behavior along with their braking behavior.

The centering error of the neighbor vehicles, its lane assignment, and its initial emergency lateral shift factor are sampled similarly to the host vehicle using equations 4.4 - 4.6. The neighbor vehicles which are assigned the same lane as the host vehicle are disregarded in the scenario simulation, as the focus of the study is only on the collisions due to the aberration of the lane-keeping functionality, causing the host vehicle to drift away from its own lane to another.

Neighbor vehicle type

The vehicle type for each neighbor vehicle for a given scenario is sampled from a discrete multi-nominal distribution as shown in equation 4.7. The probability of each vehicle type is assumed for the purpose of this study, without contradiction, as listed in table 4.7.

$$N_{typ, \beta} \sim \mathcal{M}_3(n; p_1, \dots, p_3) \forall \beta \quad (4.7)$$

$$\{ \beta \in \text{All neighbors} : n_{Lane, \beta} \neq n_{Lane, E} \}$$

Neighbor vehicle type, $N_{typ, \beta}$		
Car	Truck/Bus	Motorbike
90.5 %	9 %	0.5 %

Table 4.7.: Likelihood of neighbor vehicle type

The nature of the neighbor vehicle is essential for the traffic model as the dimensions of each of the vehicle types are drastically different from each other as shown in table 4.8, where these

average dimensions are assumed to be the same for all vehicles of the same vehicle type. And this consequently influences the relative distances between the vehicles in the simulation.

Dimension	Vehicle type, $N_{typ, \beta}$		
	Car	Truck/Bus	Motorbike
Wheelbase, WB	5 m	9 m	1.9 m
Track width, TW	2 m	2.6 m	1 m
Mass, m	1032 kg	1.2×10^4 kg	175 kg

Table 4.8.: *Dimensions of different vehicle types*

Neighbor time headway

The neighbor time headway, $t_{HW, \beta}$, is sampled at random from a gamma distribution for each neighbor vehicle as given by equation 4.8. The gamma distribution parameters are estimated by fitting the measured relative distances of a vehicle from the host vehicle in the time headway metric for a random subset of data from BMW campaigns. Figure 4.3 indicates a time headway distribution that is derived based on the trend observed from the analysis of data from BMW Campaigns. It is assumed, without contradiction, that this distribution can be adapted for all highway traffic scenarios.

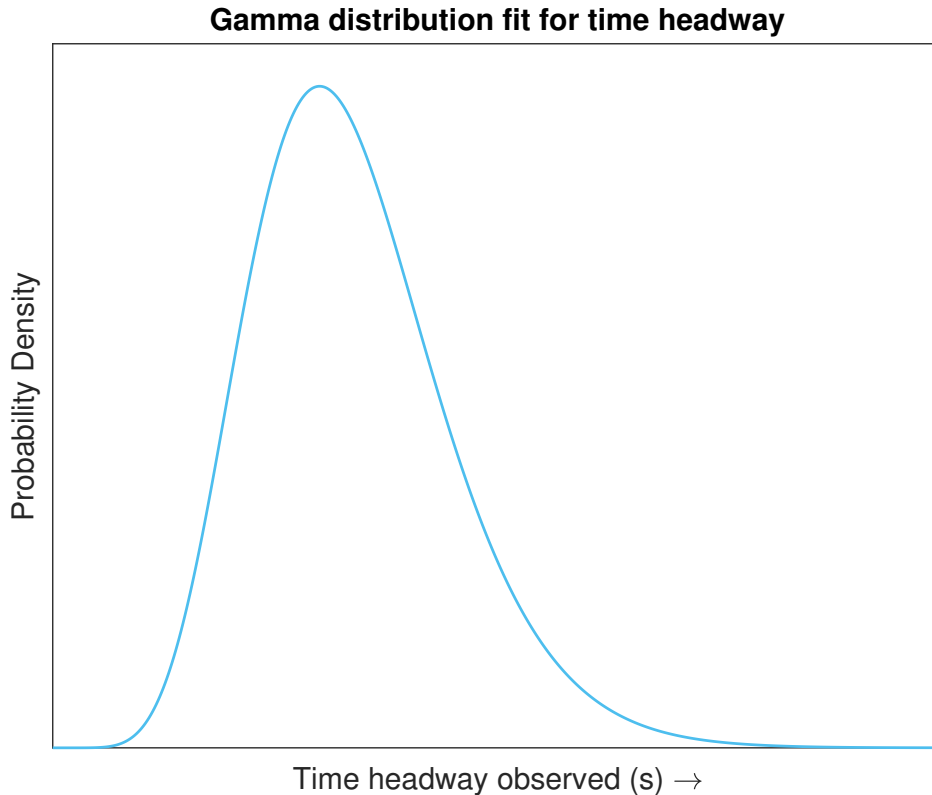


Figure 4.3.: *Distribution of distance to the vehicle ahead as a measure of time headway*

$$t_{HW, \beta} \sim \Gamma (a, b) \forall \beta \quad (4.8)$$

$$\{ \beta \in \text{All neighbors} : n_{Lane, \beta} \neq n_{Lane, E} \}$$

Initial lane-wise longitudinal position

The initial longitudinal position of the first neighbor vehicle, $q = 1$, on every lane, is denoted as $d_{0, n_{Lane,l}}$. It is assumed, without contradiction, that the initial longitudinal position of the first neighbor on every lane is positioned within 10 meters from the initial longitudinal position of the host vehicle and it is sampled from a uniform distribution as given in equation 4.9.

$$d_{0, n_{Lane,l}} \sim \mathcal{U} (0, 10) \forall l$$

$$\{ l \in \text{All lanes} : n_{Lane,l} \neq n_{Lane,E} \}$$
(4.9)

Initial lane-wise neighbor velocity

The magnitude of the relative velocity of the neighbor vehicles with respect to the host vehicle is sampled separately for the two driving modes. A uniform distribution is used for $D_{Mode, EC}$, as the velocities of all vehicles during an emergency corridor situation are in a comparable range and it is assumed as ± 5 kmph. For $D_{Mode, ND}$, a multi-nominal distribution based on a relative velocity matrix indicating the likelihood of discrete relative velocity values of the neighbor vehicle corresponding to the velocity of the host vehicle for each discrete velocity of the host vehicle. The relative velocity matrix as listed in table A.1, is an assumed distribution derived based on the trend observed from BMW campaigns, indicating the likelihood of each relative velocity of the neighboring vehicle for each discrete velocities of the reference vehicle recording the data.

In the simulation model, the initial velocities of all the neighbors along a lane regardless of the vehicle type are considered to be the same. Therefore, the initial relative velocities of the neighbor are sampled lane-wise for each scenario corresponding to the host velocity. It is assumed, without any further contradiction, that the initial velocity of neighbor vehicles in the simulation can be both slower or faster than the host vehicle. Thus, the sign of the relative velocity for each lane is sampled using an equal chance bi-nominal distribution.

$$\delta v_{0, n_{Lane,l}} \sim \begin{cases} \mathcal{B} (n; 0.5) * \mathcal{U} (0, 5), & \text{if } D_{Mode, EC} \\ \mathcal{B} (n; 0.5) * \mathcal{M}_{k, v_{0, E}} (n; p_1, \dots, p_k), & \text{if } D_{Mode, ND} \end{cases} \forall l$$

$$\{ l \in \text{All lanes} : n_{Lane,l} \neq n_{Lane,E} \}$$
(4.10)

The initial velocity of the neighbors is assigned to the neighbors in the simulation as described in equation 4.11.

$$v_{0, \beta} = v_{0,E} + \delta v_{0, n_{Lane,l}}, \quad \forall \beta$$

$$\{ \beta \in \text{All neighbors: } n_{Lane,\beta} = n_{Lane,l} \ \& \ n_{Lane,\beta} \neq n_{Lane,E} \}$$
(4.11)

Driver brake reaction time

The braking behavior of the neighbor vehicle is characterized by the driver brake reaction time, $t_{RT, \beta}$, which is the time taken by the driver to decelerate the vehicle from the perception of an immediate threat. Lane intrusion due to the KLE is characterized as a surprise event based on the results [48, 49, 50], as there is no indication to the neighbor driver via indicator or brake light signal about the lane intrusion of the host vehicle. The reaction times are generally represented as gamma distributions, so a gamma distribution is used for sampling the driver brake reaction time in this traffic model. As an exact fit of the results of [48] using a gamma curve was not possible, so for the purpose of this thesis work a trade-off between the deviation in the fitting of the 50th and 95th percentile value was considered. The driver reaction time is assumed, without any further contradiction, to be a gamma distribution having a cumulative distribution as shown in figure 4.4.

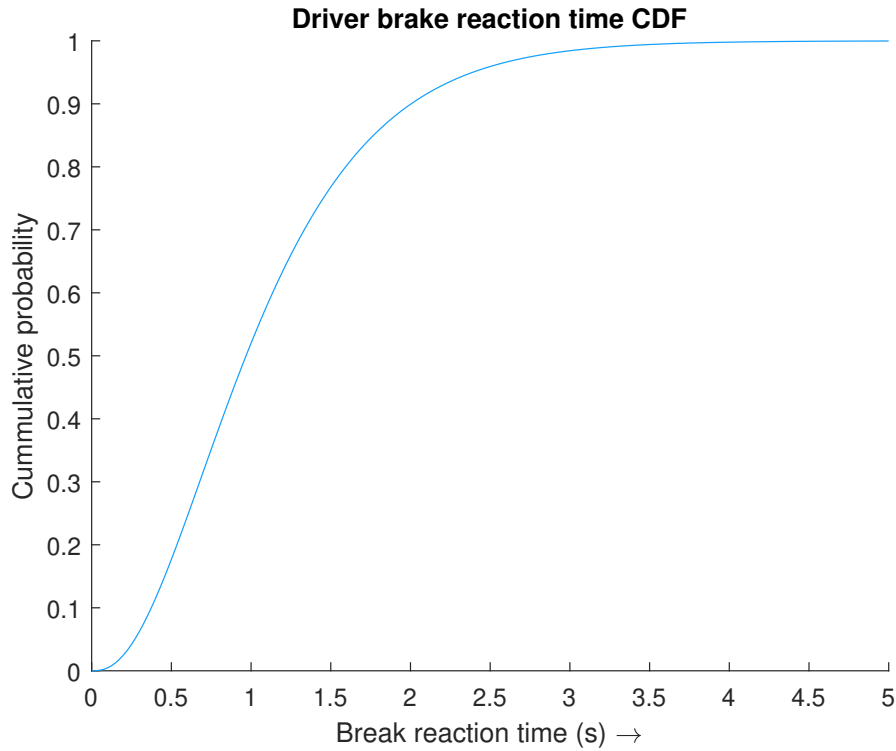


Figure 4.4.: *Estimated gamma distribution for driver brake reaction time*

The sampling of the driver brake reaction time is as shown in equation 4.12.

$$\begin{aligned}
 t_{RT, \beta} &\sim \Gamma (2.68, 0.41169) \forall \beta \\
 \{ \beta \in \text{All neighbors} : n_{Lane, \beta} \neq n_{Lane, E} \} &
 \end{aligned}
 \tag{4.12}$$

5. Results and Discussion

5.1. Traffic model simulation

5.1.1. Traffic model simulation overview

Simulation of the AD function in highway traffic conditions is very complex in nature and so the first and foremost step is to define all of the boundary conditions and the bounding box of the functional scenario that is to be simulated. The next important step is to systematically break down the functional scenario into a multi-layered rule-based logical model such that every sequential decision involved in the simulation is based on the logic inferred from expert knowledge, literature studies, and/or from expected driving behavior. And the final crucial step is to develop a mathematical model which can track the trajectories of the traffic participants as it is essential to determine the relative positioning and relative distances of the host vehicle with respect to the other traffic participants and also with respect to the road infrastructure. Figure 5.1 provides an overview of the workflow of the traffic simulation model.

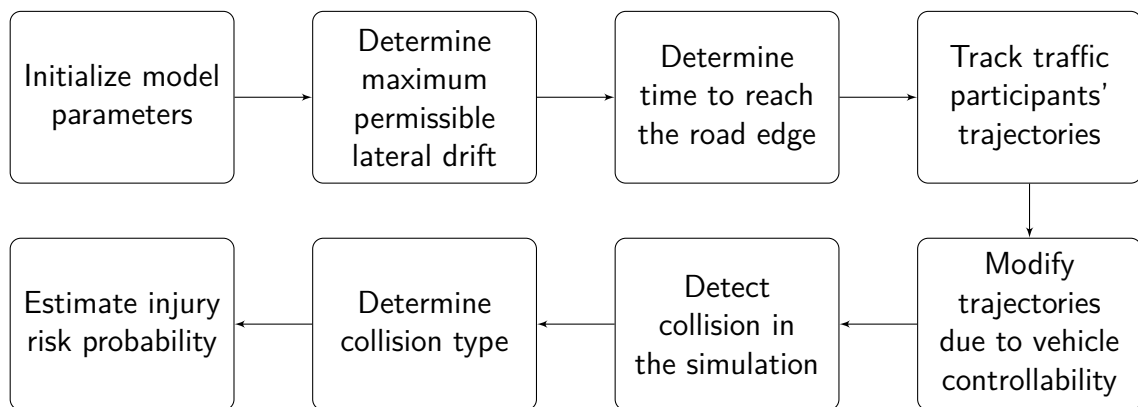


Figure 5.1.: *Workflow of the traffic simulation model*

The model workflow begins with the parameter initialization, which is the sampling of the model input parameters. After which the traffic model determines the maximum permissible lateral drift for the host vehicle along the KLE drift direction and the time required to cover this permissible lateral drift. The aim of the simulation is to determine the probability of collision and its injury level due to KLE in L3 Function, thus the model is simulated only until either the host vehicle reaches the edge of the road or the sampled KLE duration, depending on whichever comes earlier for each scenario. As the next step, the model determines the individual trajectories of all the vehicles in a scenario for the entire duration of the simulation and then identifies if the host vehicle has a collision with any of the other neighboring vehicles. In case of a potential collision, the logic for neighbor vehicle braking along with ASC function is checked for every instant of the simulation to determine whether braking is necessary for the host and/or the neighbor vehicle(s). With the updated trajectories, the model once again

checks for potential collisions between the host vehicle and the neighbors. Based on the trajectories of the vehicles, the positioning of the vehicles, and collision detection, the model then determines the type of collision. This is important to formulate injury risk functions that can estimate the injury risk probabilities for the different collisions. The traffic simulation model is iterated multiple times for different combinations of the model input parameters which are sampled at random, based on their distributions described in chapter 4 using MCS methodology. The mean value from the multiple iterations is the overall injury estimation for L3 Function in the context of lane-keeping failure.

5.1.2. Traffic model visualization

The traffic simulation model described in this thesis work is developed on the Matlab platform. To visualize the traffic scenarios simulated in the model, the trajectories of each traffic participant's center along with the road infrastructure with respect to the inertial reference frame of the traffic model are depicted in figure 5.2. It describes a traffic scenario in a four-laned road, having the curvature of the road towards the right, comprising of two neighbor vehicles driving along the road on their designated lanes where the host vehicle starts to drift towards the left side of the road due to KLE. The instant at which the neighbor vehicle 1 collides with the host vehicle is given by t_C , and $t_{B,E}$ is the instant when the necessary conditions for the ASC function are satisfied and the host vehicle begins to decelerate to avoid a side-way collision with neighbor vehicle 1.

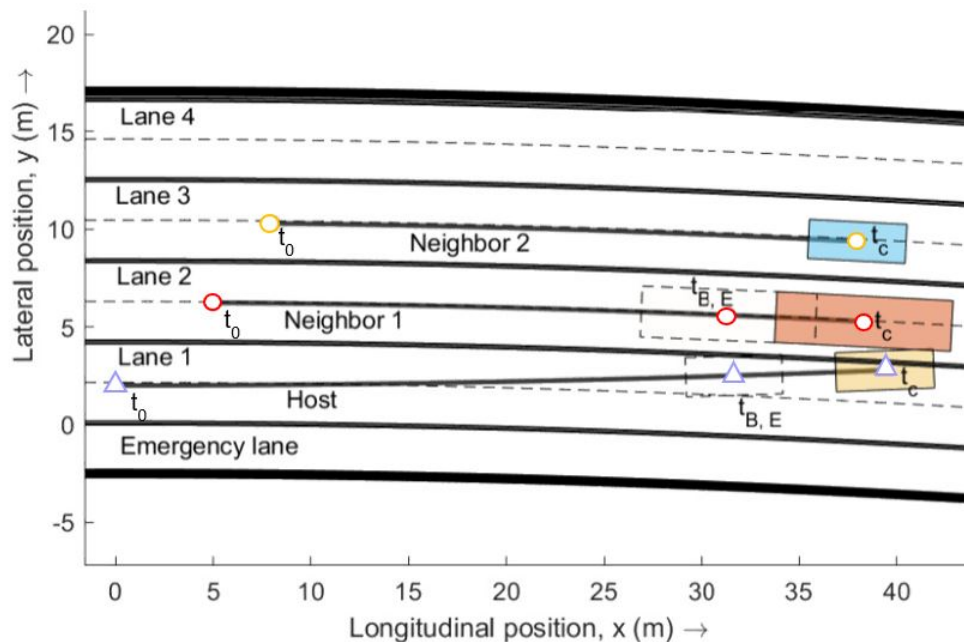


Figure 5.2.: Traffic simulation model visualization in MATLAB

The change of velocity of all the vehicles in the scenario under discussion over time is indicated in figure 5.3. Here the velocity of the host vehicle alone is reduced during the simulation because in the given scenario conditions for the ASC function alone are satisfied. The braking

of the vehicle is modelled as a reduction of the speed at a constant deceleration rate. As soon as the braking conditions are no longer satisfied, the deceleration of the individual vehicles stops.

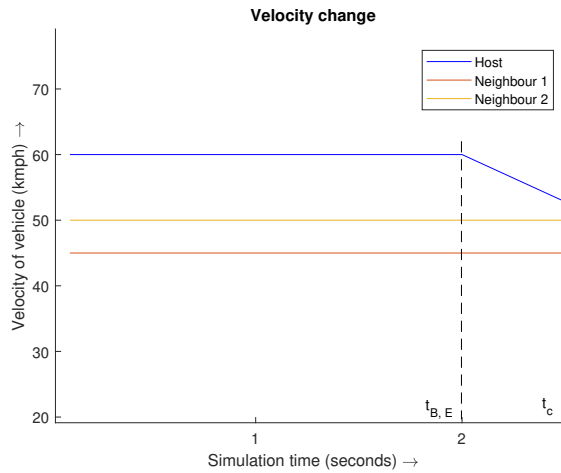
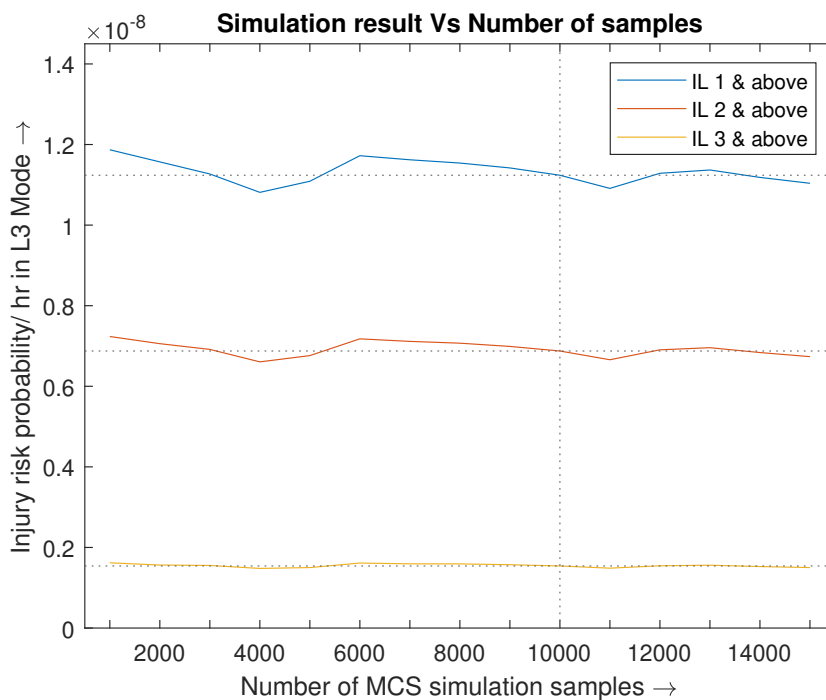


Figure 5.3.: Velocity of the vehicle during simulation

5.2. Simulation results

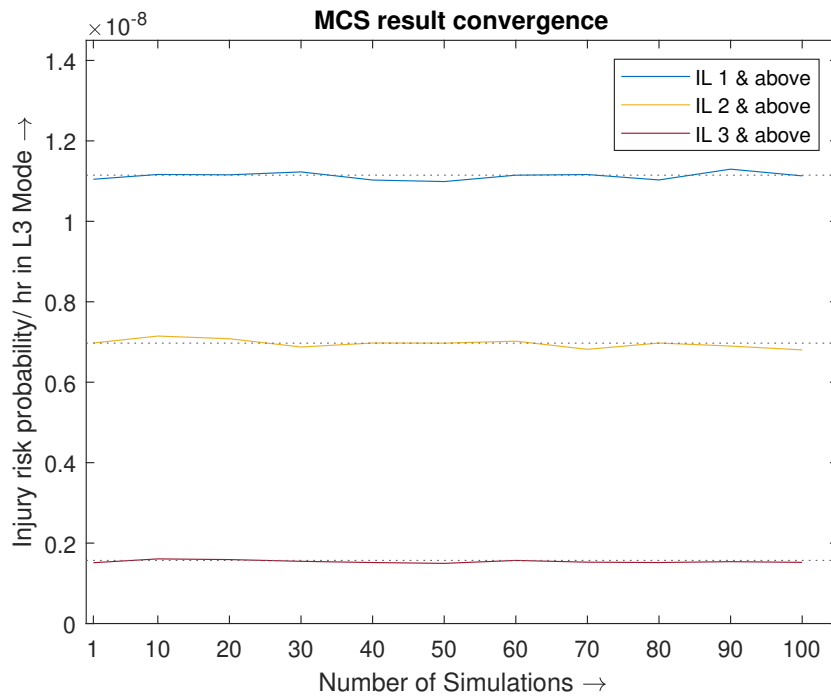
The injury risk of L3 Function due to KLE is determined using a MCS of the highway traffic model. The overall injury estimation is the weighted average of injury risk over the entire ODD, depending on its collision probability. It is assumed, without contradiction, that the exposure rate of KLE is every 3000 hours. The accuracy of the MCS result is dependent on



(a) Simulation result fluctuations Vs Number of simulation samples

Figure 5.4.: Convergence of MCS

the number of sampling points, as the variance of the result reduces by a factor of the number of random samples considered in the simulation, thereby increasing the accuracy.



(b) MCS result precision for 10,000 simulation samples

Figure 5.4.: *Convergence of MCS (conti.)*

The fluctuation of the overall injury estimation of different injury levels, based on the MCS of the traffic model, with respect to the number of random samples points for the model's input parameters considered in the simulation, is depicted in figure 5.4(a). It is evident that the degree of fluctuations reduces as the number of samples increases. Furthermore, it can also be inferred from the trend that MCS having a higher number of samples tends to oscillate and average its result around 10,000 samples. The MCS results of the traffic model stabilizes with reasonable precision for simulations that use 10,000 samples, as shown in figure 5.4(b). Hence, the traffic simulation model proposed in this thesis work delivers results with reasonable precision and accuracy while using 10,000 samples. The corresponding overall injury estimation of L3 Function is as summarized in table 5.1.

Number of samples	Error frequency, f_{KLE} (1/hr)	Injury risk probability of L3 Function ($10^{-8}/hr$)		
		IL1 & above	IL2 & above	IL3 & above
10,000	1/3000	1.10804	0.67723	0.15119

Table 5.1.: *Traffic model simulation results*

It is important to note that the model input parameters are sampled based on empirical and/or hypothesized distributions specific to the assumed ODD of the L3 Function. This ensures that most, if not all, of the scenarios generated by the combination of random input samples, are

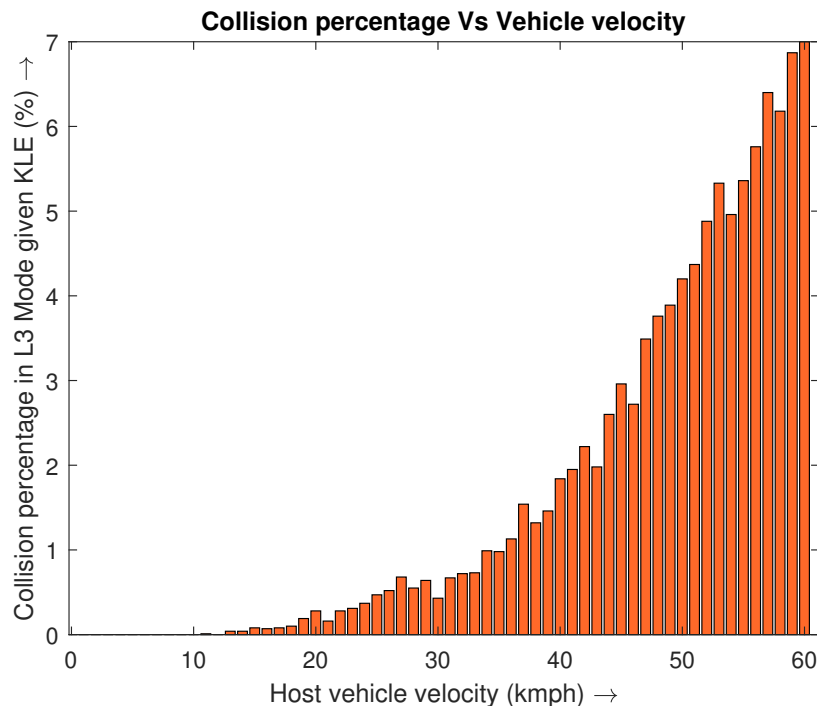
relevant and contribute to the final result. However, further improvements in the accuracy of the results are possible by implementing the concept of either importance sampling or stratified sampling.

5.3. Discussion

The highway traffic model described in this thesis work comprises a number of parameters that are necessary to completely define the scenario, as discussed in chapter 4. Each of the parameters has an effect on the injury risk of the L3 Function. This section provides a detailed discussion of the influence of specific hypothesized and empirical distributions of input parameters on the estimated injury risk. The inferences gained from understanding the dependencies of these parameters on the injury risk are essential for statistically defining a tolerable limit for each hypothesized parameter, in order to establish the safety goals for the L3 Function. To study the individual effects of a parameter on the injury risk, the traffic model is simulated for 10,000 randomized sample points, generating different combinations of traffic scenarios through MCS methodology. The model input parameters are sampled as described in chapter 4, except for the parameter under examination.

5.3.1. Injury risk Vs v_0, E

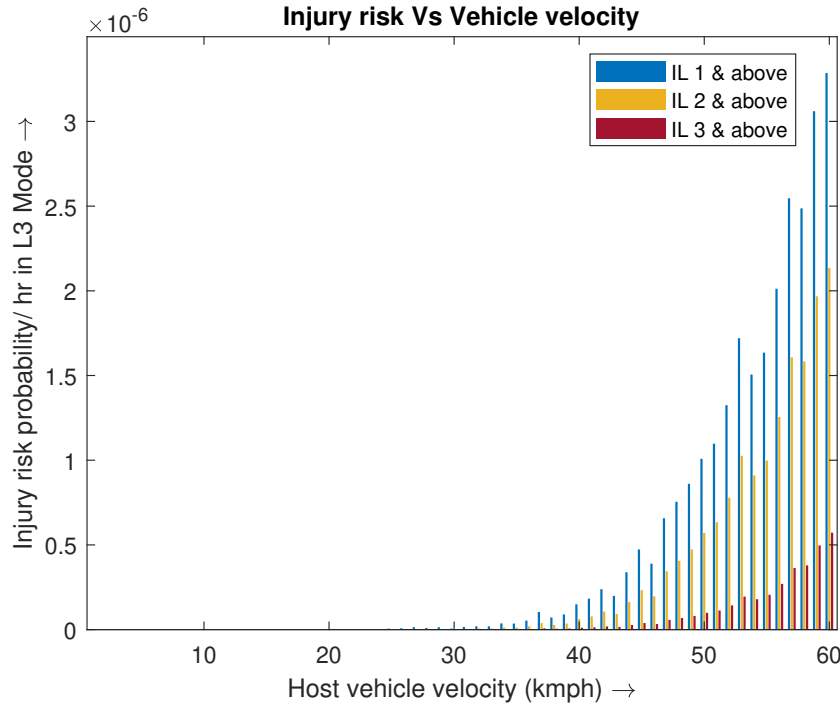
The velocity of the vehicle is directly proportional to the collision probability of the L3 Function vehicle, given a KLE, as shown in figure 5.5(a). The distance covered by the vehicle both



(a) Collision percentage with vehicle velocity

Figure 5.5.: Injury risk trend with vehicle velocity

longitudinally and laterally increases, as the velocity of the vehicle increases. This increased distance can cause the vehicle to leave the road and collide with the road edge hazards. As the distance traveled by the L3 Function vehicle, given a KLE, increases, the likelihood of collision also increases. It is important to note that the highest percentage of collision observed in the simulations is lower than 7%, indicating that the likelihood of a collision arising from the lane-keeping failure is extremely low, given that the extreme characteristics of the KLE are within the specified bounds.



(b) Injury probability with vehicle velocity

Figure 5.5.: Injury risk trend with vehicle velocity (conti.)

The average injury estimation of the host vehicle for each specific velocity in L3 Function, given a KLE, is shown in figure 5.5(b). As expected, the trend of the injury risk probabilities is also directly proportional to the host vehicle velocity. This is because the injury risk functions depend on the impact velocity, in addition to the collision percentage. Notably, the injury risk values are very low or even negligible for velocities up to 35 kmph and begin to increase steeply thereafter.

5.3.2. Injury risk Vs f_{KLE}

As expected, the injury probability decreases drastically with the decrease in f_{KLE} , as seen in figure 5.6. The relation between the injury risk and failure rate is linear, as the overall injury estimation is the mean injury risk from the MCS of the traffic model weighted by the occurrence rate of the failure. Based on the injury probability arising from different error frequencies, the safety goal of L3 Function in terms of acceptable lane-keeping failure frequency

can be defined. This ensures that the injury probability, based on the current accident statistics is on a comparable scale to the injury estimation of L3 Function arising from KLE.

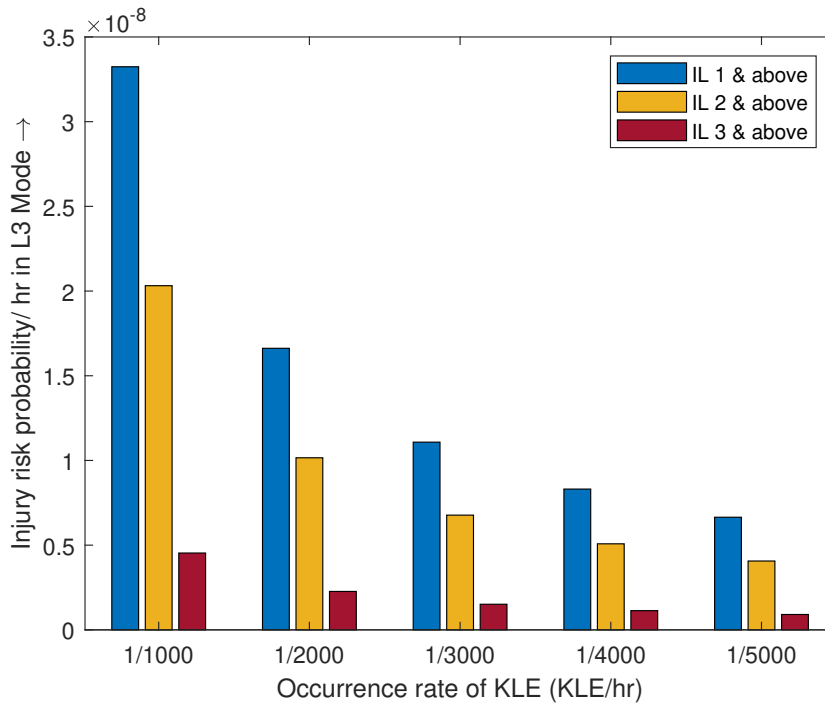


Figure 5.6.: Injury risk trend with KLE occurrence rate

5.3.3. Injury risk Vs t_{KLE}

The effect of t_{KLE} on the injury probability is very straightforward as with the increase in the duration, the probability of collision also increases. Multiple iterations of the traffic

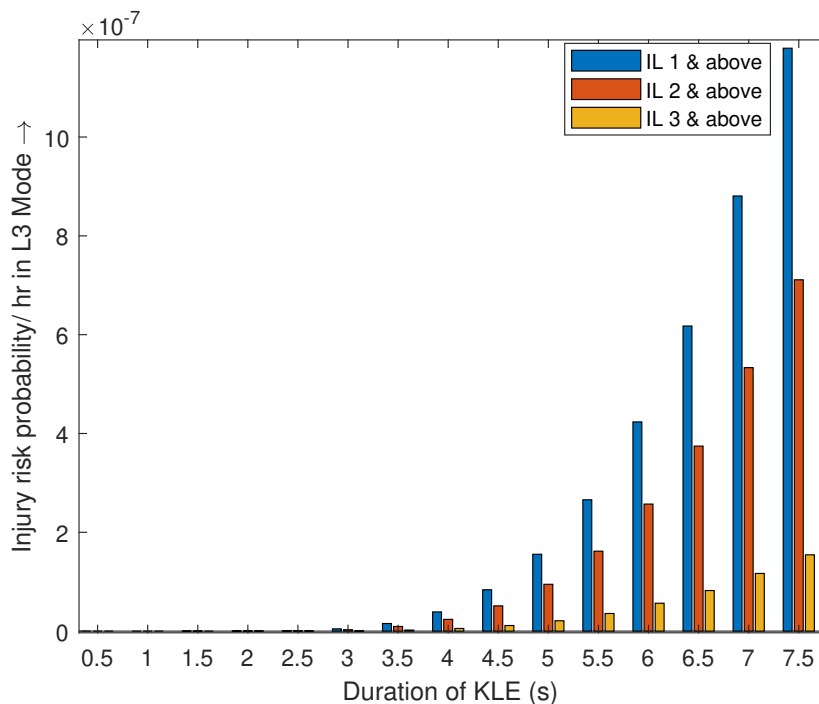


Figure 5.7.: Injury risk trend with KLE duration

model are simulated by fixing only the KLE duration parameter in order to study its influence. The exponential increase in the trend is due to the combined effect of the higher collision rate observed at higher velocities, as explained in section 5.3.1, along with the effect of the increase in error duration for each simulation, leading to an overall increase in the collision probability. Based on the trend of the injury risk with respect to the error duration, the safety goal of the L3 Function in terms of acceptable duration for lane-keeping error can be defined.

5.3.4. Injury risk Vs r_{KLE}

The effect of the r_{KLE} on the injury risk is not linear, as shown in figure 5.8. Evidently, the injury risk is very high for a low drift radius. This is because the probability distribution of the road curvature indicates a higher likelihood of very large road curvatures, implying straighter roads. When combined with a very small KLE drift radius, it leads to a significant lateral drift of the automated vehicle during KLE, resulting in the collision of the automated vehicle with either the neighboring vehicle or road edge hazards. As the drift radius increases, the automated vehicle is more likely to follow a relatively straighter path compared to the road curvature, resulting in an oscillating trend for the overall lateral drift as the KLE drift radius increases. A similar trend can be observed in the injury risk as the KLE drift radius increases.

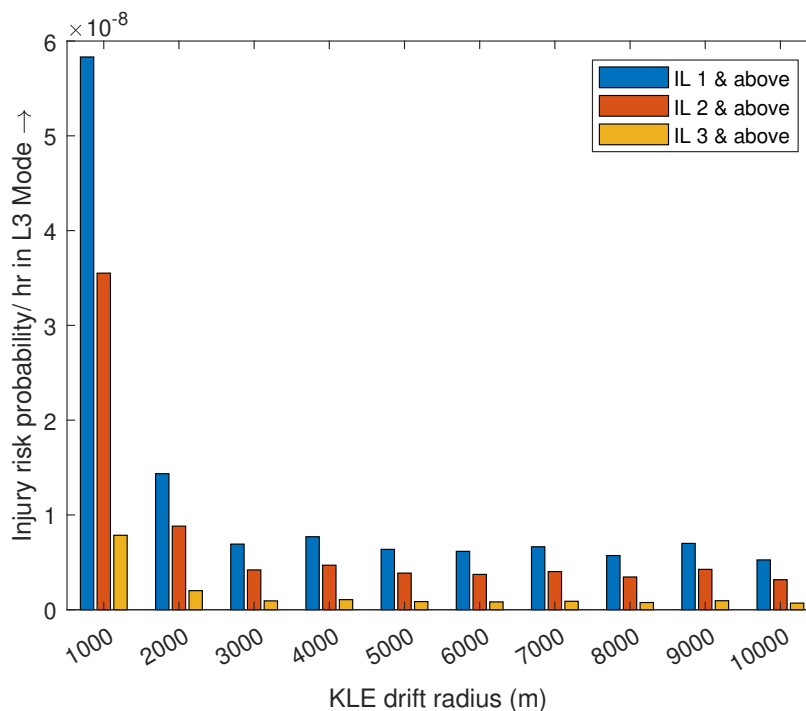


Figure 5.8.: Injury risk trend with KLE drift radius

The inferences from this trend are not straightforward, and it is not possible to directly adopt these interpretations to establish a tolerable limit for the KLE drift radius. This is because the measurement of the drift radius is with respect to an inertial reference in the traffic model, and it is not relative to the road curvature.

5.3.5. Injury risk Vs $t_{HW, \beta}$

The influence of $t_{HW, \beta}$ on the injury risk is shown in figure 5.9. It can be inferred that the time headway of the neighbor alone does not influence the injury risk in an impactful manner. The reduction in the distance between the neighbor doesn't necessarily lead to a collision between the host vehicle and the neighbor. This is because there are multiple lanes available in a traffic scenario, and the densely populated lane doesn't necessarily have to be the immediate lane of the host vehicle.

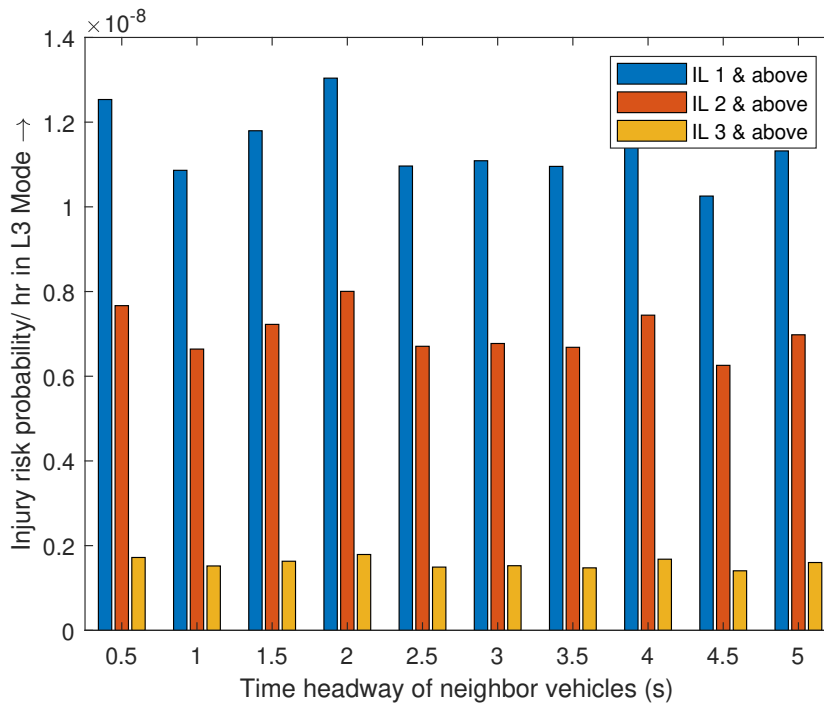


Figure 5.9.: *Injury risk trend with KLE duration*

One of the most influential characteristics of the neighboring vehicles in the injury estimation of lane-keeping failure for an automated vehicle is the traffic density. Traffic density is introduced into the proposed highway traffic model using a combination of the different input parameters, such as the relative velocity of the neighbors, the number of neighboring road users, the distance between the two neighbor vehicles, and the starting position of the neighbor vehicles with respect to the automated vehicle. Therefore, these parameters individually would not significantly influence the injury estimation of an automated vehicle due to lane-keeping failure. Nevertheless, the combined effects of these parameters are innately incorporated into MCS of the proposed highway traffic model described in this thesis work.

6. Conclusion and Future work

6.1. Conclusion

This thesis contributes to the SOTIF analysis of a highly automated driving function, specifically the L3 Function, by quantifying the safety risk of the function while considering the deviation or failure of the lane-keeping functionality of the system. The primary focus of this thesis is on assessing the safety risk resulting from the failure of the function, rather than investigating the cause of the failure. Due to the challenges and limitations of conducting vehicle testing during the development phase, the proposed risk quantification method in this work is based on simulations of lane-keeping failure in various highway traffic scenarios. The safety assessments carried out by simulations are both prospective and statistically significant, owing to their data-driven approach.

For the simulation of the lane-keeping failure, a structured methodology is defined in this thesis. The goal is to create a highly parameterized highway traffic model that can simulate the interactive behavior of an automated vehicle equipped with the L3 Function experiencing a lane-keeping failure, as well as the interactive behavior of manually driven vehicles by other road users in the traffic scenario. The objective is to determine the probability of collision and the severity of injuries resulting from these collisions using the MCS methodology.

The overall injury estimation results from the simulation of the highway traffic model described in this thesis work are well within the tolerable limits based on the MEM principle. The comparative study of the influence of different traffic scenario parameters on safety risk indicates that the velocity of the vehicle has the most significant impact, followed by the duration of the failure, and then the failure occurrence rate. These individual trends aid in establishing tolerable limits for each of the parameters that define lane-keeping failure behavior.

The framework established in this thesis work is built on assumptions that are justified based on the available knowledge and understanding of lane-keeping errors in automated vehicles. These assumptions form the basis for creating the traffic model and conducting simulations. However, it is important to acknowledge that these assumptions may not fully capture the complexity of real-world scenarios and could potentially introduce biases or inaccuracies in the results. Furthermore, the data used in the current work are sourced from literature references and various BMW campaigns. Even though these sources provide valuable insights into the highway traffic scenario comprehension, it is important to acknowledge that the results may not be 100% reliable. The data obtained from the literature might be based on specific conditions or experimental setups that may not fully represent all of the real-world scenarios. Similarly, the data collected from BMW campaigns might be influenced by specific driving conditions,

limiting the ability to generalize the findings to a broader context.

To address these limitations, future research could consider expanding the data collection to include a more diverse range of sources and real-world driving scenarios. Conducting extensive field studies could enhance both scenario comprehension and data credibility, thereby increasing the reliability and generalizability of the results. By acknowledging the limitations of the study and identifying the opportunities for improvement, the thesis work establishes a solid foundation for further advancements in the simulation of lane-keeping failure in automated vehicles.

6.2. Future work

The objectives of the thesis were successfully achieved by developing a methodology to quantify the risk of lane-keeping failure in automated vehicles using a parameterized highway traffic model. However, there are several potential avenues for further extension and exploration, as discussed below.

- *Refine model parameters:* The legitimacy of the highway traffic model can be enhanced by refining the model parameters through the incorporation of more empirical data. Rather than relying solely on hypothesized distributions, the utilization of empirical data can provide more accurate representations of the model parameters when generating random samples using MCS.
- *Interactive behavior:* Incorporating all possible collision mitigation behavior of the road users, such as steering, acceleration, braking, and combinations thereof, into the traffic model.
- *Wider risk assessment scope:* Inclusion of injury risk from all road users directly involved in a collision, as well as the road users who are passively affected by the collision, while quantifying the risk of the L3 Function.
- *Piecemeal failure modelling:* Consideration of the lane-keeping failure as an error that is introduced into the traffic model intermittently and erratically over a period of time, rather than introducing the error as a constant value throughout the failure duration.
- *Special collision cases:* Integrating additional special collision cases for automated vehicles in the context of keep lane failure, such as collisions with a lane divider, collisions near exit lanes, collisions with road obstacles, collisions with cyclists, etc.
- *Broadening the operating domain:* Expanding the scope of the automated driving function to include urban traffic conditions when estimating the safety risk of highly automated driving function. Furthermore, the proposed traffic model can be further expanded to also include higher-level automated driving functions.

Bibliography

1. MALLOZZI, Piergiuseppe; PELLICCIONE, Patrizio; KNAUSS, Alessia; BERGER, Christian; MOHAMMADIHA, Nassar. Autonomous vehicles: state of the art, future trends, and challenges. *Automotive systems and software engineering: State of the art and future trends*. 2019, pp. 347–367.
2. *USDOT Releases 2016 Fatal Traffic Crash Data* [National Highway Traffic Safety Administration]. 2017. <https://www.nhtsa.gov/press-releases/usdot-releases-2016-fatal-traffic-crash-data>.
3. KALRA, Nidhi; GROVES, David G. *The Enemy of Good: Estimating the Cost of Waiting for Nearly Perfect Automated Vehicles*. Santa Monica, CA: RAND Corporation, 2017. Available from DOI: 10.7249/RR2150.
4. FAGNANT, Daniel; KOCKELMAN, Kara. Preparing a nation for autonomous vehicles: Opportunities, barriers and policy recommendations. *Transportation Research Part A: Policy and Practice*. 2015, vol. 77. Available from DOI: 10.1016/j.tra.2015.04.003.
5. VAHIDI, Ardalan; SCIARRETTA, Antonio. Energy saving potentials of connected and automated vehicles. *Transportation Research Part C: Emerging Technologies*. 2018, vol. 95, pp. 822–843. ISSN 0968-090X. Available from DOI: <https://doi.org/10.1016/j.trc.2018.09.001>.
6. WANG, Jun; ZHANG, Li; HUANG, Yanjun; ZHAO, Jian; BELLA, Francesco. Safety of autonomous vehicles. *Journal of advanced transportation*. 2020, vol. 2020, pp. 1–13.
7. NALIC, Demin; MIHALJ, Tomislav; BÄUMLER, Maximilian; LEHMANN, Matthias; EICHBERGER, Arno; BERNSTEINER, Stefan. Scenario based testing of automated driving systems: A literature survey. In: *FISITA web Congress*. 2020, vol. 10.
8. TAXONOMY, SAE. Definitions for terms related to driving automation systems for on-road motor vehicles. Publication J3016_202104. *Society of Automotive Engineers*. 2021.
9. NHTSA. *Automated Vehicles for Safety, United States Department of Transportation*. 2019. Available also from: <https://www.nhtsa.gov/technology-innovation/automated-vehicles-safety#nhtsa-action>.
10. TAŞ, Ömer Şahin; KUHNT, Florian; ZÖLLNER, J. Marius; STILLER, Christoph. Functional system architectures towards fully automated driving. In: *2016 IEEE Intelligent Vehicles Symposium (IV)*. 2016, pp. 304–309. Available from DOI: 10.1109/IVS.2016.7535402.
11. RUSSELL, Stuart J. *Artificial intelligence a modern approach*. Pearson Education, Inc., 2010.

12. ILAS, Constantin. Electronic sensing technologies for autonomous ground vehicles: A review. In: *2013 8th International Symposium on Advanced Topics in Electrical Engineering (ATEE)*. IEEE, 2013, pp. 1–6.
13. TAKÁCS, Árpád; DREXLER, Dániel András; GALAMBOS, Péter; RUDAS, Imre J.; HAIDEGGER, Tamás. Assessment and Standardization of Autonomous Vehicles. In: *2018 IEEE 22nd International Conference on Intelligent Engineering Systems (INES)*. 2018, pp. 000185–000192. Available from DOI: 10.1109/INES.2018.8523899.
14. JUNIETZ, Philipp; WACHENFELD, Walther; KLONECKI, Kamil; WINNER, Hermann. Evaluation of Different Approaches to Address Safety Validation of Automated Driving. In: *2018 21st International Conference on Intelligent Transportation Systems (ITSC)*. 2018, pp. 491–496. Available from DOI: 10.1109/ITSC.2018.8569959.
15. WINNER, Hermann; HAKULI, S.; LOTZ, F.; SINGER, Christina. *Handbook of driver assistance systems: Basic information, components and systems for active safety and comfort*. 2015. Available from DOI: 10.1007/978-3-319-12352-3.
16. WINNER, Hermann; WACHENFELD, Walther; JUNIETZ, Phillip. Validation and Introduction of Automated Driving. In: *Automotive Systems Engineering II*. Ed. by WINNER, Hermann; PROKOP, Günther; MAURER, Markus. Cham: Springer International Publishing, 2018, pp. 177–196. ISBN 978-3-319-61607-0. Available from DOI: 10.1007/978-3-319-61607-0_8.
17. MARTIN, Helmut; TSCHABUSCHNIG, Kurt; BRIDAL, Olof; WATZENIG, Daniel. Functional Safety of Automated Driving Systems: Does ISO 26262 Meet the Challenges? In: *Automated Driving: Safer and More Efficient Future Driving*. Ed. by WATZENIG, Daniel; HORN, Martin. Cham: Springer International Publishing, 2017, pp. 387–416. ISBN 978-3-319-31895-0. Available from DOI: 10.1007/978-3-319-31895-0_16.
18. KÖLBL, Martin; LEUE, Stefan. Automated functional safety analysis of automated driving systems. In: *Formal Methods for Industrial Critical Systems: 23rd International Conference, FMICS 2018, Maynooth, Ireland, September 3-4, 2018, Proceedings 23*. Springer, 2018, pp. 35–51.
19. BERGENHEM, Carl; JOHANSSON, Rolf; SODERBERG, Andreas; NILSSON, Jonas; TRYGGVESSON, Jörgen; TÖRNGREN, Martin; URSING, Stig. How to Reach Complete Safety Requirement Refinement for Autonomous Vehicles. 2015.
20. FULLER, Ray. Towards a general theory of driver behaviour. *Accident Analysis Prevention*. 2005, vol. 37, no. 3, pp. 461–472. ISSN 0001-4575. Available from DOI: <https://doi.org/10.1016/j.aap.2004.11.003>.
21. CHU, Jiayun; ZHAO, Tingdi; JIAO, Jian; YUAN, Yuan; JING, Yongfeng. SOTIF-Oriented Perception Evaluation Method for Forward Obstacle Detection of Autonomous Vehicles. *IEEE Systems Journal*. 2023, pp. 1–12. Available from DOI: 10.1109/JSYST.2023.3234200.

22. GYLLENHAMMAR, Magnus; JOHANSSON, Rolf; WARG, Fredrik; CHEN, DeJiu; HEYN, Hans-Martin; SANFRIDSON, Martin; SODERBERG, Jan; THORSÉN, Anders; URSING, Stig. Towards an Operational Design Domain That Supports the Safety Argumentation of an Automated Driving System. In: 2020.
23. KHATUN, Marzana; GLASS, Michael; JUNG, Rolf. Scenario-based Extended HARA Incorporating Functional Safety & SOTIF for Autonomous Driving. In: BARALDI, Piero (ed.). *E-proceedings of the 30th European Safety and Reliability Conference and 15th Probabilistic Safety Assessment and Management Conference*. 2020, vol. 2020, pp. 53–59. (ESREL2020 PSAM15) ; 01 - 05 November 2020 Venice, Italy. Available also from: <https://www.rpsonline.com.sg/proceedings/esrel2020/html/5225.xml>.
24. AMERSBACH, Christian; RUPPERT, Timm; HEBGEN, Niclas; WINNER, Hermann. Macroscopic Safety Requirements for Highly Automated Driving in Urban Environments. In: Graz, 2021, pp. 1–14. Available from DOI: <https://doi.org/10.26083/tuprints-00013470>. Veranstaltungstitel: 13. Graz Symposium Virtual Vehicle (GSVF).
25. KUHLMANN, A. Einführung in die Sicherheitstechnik (Introduction into Safety Technology), Friedr. Vieweg & Sohn, Verlag TÜV Rheinland. 1981.
26. JUNIETZ, Philipp; STEININGER, Udo; WINNER, Hermann. Macroscopic safety requirements for highly automated driving. *Transportation research record*. 2019, vol. 2673, no. 3, pp. 1–10.
27. DI FABIO, Udo; BROY, Manfred; BRÜNGGER, RJ; EICHHORN, Ulrich; GRUNWALD, Armin, et al. Ethics commission automated and connected driving. *Federal Ministry of Transport and Digital Infrastructure of the Federal Republic of Germany*. 2017, vol. 1.
28. KAUFFMANN, Nina; FAHRENKROG, Felix; DREES, Ludwig; RAISCH, Florian. Positive risk balance: a comprehensive framework to ensure vehicle safety. *Ethics and Information Technology*. 2022, vol. 24, no. 1, p. 15.
29. KRENN, Andreas; STÖKL, Alexander; WEBER, Nina; BARUP, Sten; WEIDL, Thorsten; HOFFMANN, André; BREDESEN, Rolv Erlend; LANNIC, Marine; MÜLLER, Stefan; STOFFELS, Nicole, et al. International Recommendations for Ice Fall and Ice Throw Risk Assessments. *Wind Energy in Cold Climates*. 2018.
30. KEELER, Paul. Notes on stochastic processes. 2018.
31. LOPEZ, Pablo Alvarez; BEHRISCH, Michael; BIEKER-WALZ, Laura; ERDMANN, Jakob; FLÖTTERÖD, Yun-Pang; HILBRICH, Robert; LÜCKEN, Leonhard; RUMMEL, Johannes; WAGNER, Peter; WIESSNER, Evamarie. Microscopic traffic simulation using sumo. In: *2018 21st international conference on intelligent transportation systems (ITSC)*. IEEE, 2018, pp. 2575–2582.
32. WACHENFELD, Walther Hans Karl. How stochastic can help to introduce automated driving. 2017.

33. ÅSLJUNG, Daniel. On statistical methods for safety validation of automated vehicles: using threat metrics to accelerate safety evidence generation. *Doktorsavhandlingar vid Chalmers tekniska högskola. Ny serie*. 2022, no. 5223.
34. ROBERT, Christian P; CASELLA, George; CASELLA, George. *Monte Carlo statistical methods*. Vol. 2. Springer, 1999.
35. BROADHURST, A.; BAKER, S.; KANADE, T. Monte Carlo road safety reasoning. In: *IEEE Proceedings. Intelligent Vehicles Symposium, 2005*. 2005, pp. 319–324. Available from DOI: 10.1109/IVS.2005.1505122.
36. GELDER, Erwin de; SABERI, A Khabbaz; ELROFAI, Hala. A method for scenario risk quantification for automated driving systems. In: *26th International Technical Conference on the Enhanced Safety of Vehicles (ESV)*. Mira Smart, 2019.
37. FENNER, Harold A; FLAMBOE, Eugene E; NELSON, Wilton D; HAMES, Lee N, et al. *Field application and research development of the abbreviated injury scale*. 1971. Tech. rep. SAE Technical Paper.
38. BAKER, Susan P; O'NEILL, Brian; HADDON JR, William; LONG, William B. The injury severity score: a method for describing patients with multiple injuries and evaluating emergency care. *Journal of Trauma and Acute Care Surgery*. 1974, vol. 14, no. 3, pp. 187–196.
39. BAKER, Susan P; O'NEILL, Brian. The injury severity score: an update. *Journal of Trauma and Acute Care Surgery*. 1976, vol. 16, no. 11, pp. 882–885.
40. PRASAD, Priya; MERTZ, Harold J; DALMOTAS, Dainius J; AUGENSTEIN, Jeffrey S; DIGGES, Kennerly. Evaluation of the field relevance of several injury risk functions. *Stapp car crash journal*. 2010, vol. 54, p. 49.
41. KOETJE, Bethany D; GRABOWSKI, Jurek G. A methodology for the geometric standardization of vehicle hoods to compare real-world pedestrian crashes. In: *Annals of Advances in Automotive Medicine/Annual Scientific Conference*. Association for the Advancement of Automotive Medicine, 2008, vol. 52, p. 193.
42. NISHIMOTO, Tetsuya; MUKAIGAWA, Kosuke; TOMINAGA, Shigeru; LUBBE, Nils; KIUCHI, Toru; MOTOMURA, Tomokazu; MATSUMOTO, Hisashi. Serious injury prediction algorithm based on large-scale data and under-triage control. *Accident Analysis & Prevention*. 2017, vol. 98, pp. 266–276.
43. ADMINISTRATION, National Highway Traffic Safety et al. Crashworthiness Data System, Data Collection, Coding, and Editing Manual. *US Department of Transportation: Washington, DC*. 2000.
44. RECHNITZER, George; LANE, John Cook; SCOTT, Gray. Rollover crash study - vehicle design and occupant injuries. In: 1996.
45. FGVS. *RMS - Richtlinien für die Markierung von Straßen* [<https://www.fgsv-verlag.de/rms-teil-a-autobahnen-fgsv-reader>]. 2019. ISBN 978-3-86446-251-1.

46. VERKEHRSWESEN (GERMANY). ARBEITSGRUPPE STRASSENENTWURF, Forschungsgesellschaft für Strassen-und. *Guidelines for the Design of Motorways: RAA*. FGSV Verlag GmbH, 2011. FGSV (Series). Available also from: <https://books.google.de/books?id=BCjxoAEACAAJ>.
47. HE, Yong-Ming; PEI, Yu-Long; RAN, Bin; KANG, Jia; SONG, Yu-Ting. Superhighway Virtual Track System Based on Intelligent Road Buttons. *IEEE Access*. 2020, vol. PP, pp. 1–1. Available from DOI: 10.1109/ACCESS.2020.2974192.
48. SUMMALA, Heikki. Brake Reaction Times and Driver Behavior Analysis. *Transportation Human Factors*. 2000, vol. 2, pp. 217–226. Available from DOI: 10.1207/STHF0203_2.
49. OLSON, Paul L.; SIVAK, Michael. Perception-Response Time to Unexpected Roadway Hazards. *Human Factors*. 1986, vol. 28, no. 1, pp. 91–96. Available from DOI: 10.1177/001872088602800110. PMID: 3710489.
50. POLIAK, Milos; SVABOVA, Lucia; BENUS, Jan; DEMIRCI, Ebru. Driver Response Time and Age Impact on the Reaction Time of Drivers: A Driving Simulator Study among Professional-Truck Drivers. *Mathematics*. 2022, vol. 10, no. 9. ISSN 2227-7390. Available from DOI: 10.3390/math10091489.

A. Appendix

Reference velocity (kmph)	Likelihood of relative velocity in kmph (%)																		
	0-5	6-10	11-15	16-20	21-25	26-30	31-35	36-40	41-45	46-50	51-55	56-60	61-65	66-70	71-75	76-80	81-85	86-90	90-95
30	5	35	15	15	10	5	0	5	0	0	5	5	0	0	0	0	0	0	0
31	10	10	20	30	10	5	0	5	0	0	0	5	0	0	5	0	0	0	0
32	15	30	10	15	20	5	0	0	0	0	5	0	0	0	0	0	0	0	0
33	10	25	15	20	10	0	0	5	5	0	5	0	5	0	0	0	0	0	0
34	0	40	30	10	5	5	0	5	0	5	0	0	0	0	0	0	0	0	0
35	15	10	45	5	15	10	0	0	0	0	0	0	0	0	0	0	0	0	0
36	10	15	15	15	10	15	0	10	10	0	0	0	0	0	0	0	0	0	0
37	15	25	20	10	15	5	0	0	5	0	0	5	0	0	0	0	0	0	0
38	5	30	20	15	15	0	0	5	0	5	0	0	5	0	0	0	0	0	0
39	10	35	20	10	15	0	10	0	0	0	0	0	0	0	0	0	0	0	0
40	5	35	5	15	15	10	0	5	0	10	0	0	0	0	0	0	0	0	0
41	10	20	15	25	5	0	5	0	0	5	0	5	0	5	0	0	5	0	0
42	20	30	30	10	10	0	0	0	0	0	0	0	0	0	0	0	0	0	0
43	10	35	20	15	5	0	0	5	0	5	5	0	0	0	0	0	0	0	0
44	5	35	15	20	5	0	0	0	15	0	0	0	0	0	0	0	5	0	0
45	10	10	35	15	10	5	5	5	0	0	0	0	0	0	0	0	0	0	0
46	0	20	0	15	10	20	10	10	10	0	5	0	0	0	0	0	0	0	0

Continued on next page

Table A.1 – continued from previous page

Reference velocity (kmph)	Likelihood of relative velocity in kmph (%)																		
	0- 5	6- 10	11- 15	16- 20	21- 25	26- 30	31- 35	36- 40	41- 45	46- 50	51- 55	56- 60	61- 65	66- 70	71- 75	76- 80	81- 85	86- 90	90- 95
47	0	15	40	10	10	10	5	5	0	5	0	0	0	0	0	0	0	0	0
48	0	20	35	15	10	10	0	10	0	0	0	0	0	0	0	0	0	0	0
49	0	15	30	15	25	0	5	0	5	0	5	0	0	0	0	0	0	0	0
50	20	15	15	10	10	5	5	5	0	0	0	0	5	0	5	5	0	0	0
51	10	20	25	15	5	15	5	0	0	0	0	0	0	5	0	0	0	0	0
52	0	35	30	25	5	5	0	0	0	0	0	0	0	0	0	0	0	0	0
53	5	20	10	30	10	5	5	5	0	5	0	0	0	0	0	0	5	0	0
54	20	15	5	15	25	10	10	0	0	0	0	0	0	0	0	0	0	0	0
55	0	30	20	10	20	15	0	0	0	0	0	0	0	0	5	0	0	0	0
56	20	20	30	0	15	7.5	7.5	0	0	0	0	0	0	0	0	0	0	0	0
57	5	40	10	20	10	5	0	0	5	5	0	0	0	0	0	0	0	0	0
58	10	15	20	15	10	0	10	0	5	0	5	5	0	0	5	0	0	0	0
59	10	35	20	10	10	0	0	0	10	5	0	0	0	0	0	0	0	0	0
60	10	15	15	35	10	5	5	0	0	5	0	0	0	0	0	0	0	0	0

Table A.1.: *Relative velocity likelihood matrix*